JGR Atmospheres

RESEARCH ARTICLE
10.1029/2019JD031814

Divergent Regional Climate Consequences of Maintaining Current Irrigation Rates in the 21st Century

Benjamin I. Cook[1,2], Sonali Shukla McDermid[3], Michael J. Puma[4], A. Park Williams[5], Richard Seager[2], Maxwell Kelley[1], Larissa Nazarenko[1], and Igor Aleinov[1]

[1]NASA Goddard Institute for Space Studies, New York, NY, USA, [2]Ocean and Climate Physics, Lamont-Doherty Earth Observatory, Palisades, NY, USA, [3]Department of Environmental Studies, New York University, New York, NY, USA, [4]Center for Climate Systems Research, Columbia University, New York, NY, USA, [5]Tree-Ring Lab, Lamont-Doherty Earth Observatory, Palisades, NY, USA

Key Points:
- Using a climate model ensemble, we evaluate irrigation effects on projected climate change-forced temperature and soil moisture trends
- Maintaining current irrigation continues moderating projected 21st century warming and drying, even as greenhouse gas forcing increases
- The magnitude of irrigation effects varies strongly by region, however, and depends heavily on the background evaporative regime

Correspondence to:
B. I. Cook,
benjamin.i.cook@nasa.gov

Citation:
Cook, B. I., McDermid, S. S., Puma, M. J., Williams, A. P., Seager, R., Kelley, M., et al. (2020). Divergent regional climate consequences of maintaining current irrigation rates in the 21st century. *Journal of Geophysical Research: Atmospheres*, *125*, e2019JD031814. https://doi.org/10.1029/2019JD031814

Received 11 OCT 2019
Accepted 1 MAY 2020
Accepted article online 13 MAY 2020

Abstract There is strong evidence that the expansion and intensification of irrigation over the twentieth century has affected climate in many regions. However, it remains uncertain if these irrigation effects, including buffered warming trends, will weaken or persist under future climate change conditions. Using a 20-member climate model ensemble simulation, we demonstrate that irrigation will continue to attenuate greenhouse gas-forced warming and soil moisture drying in many regions over the 21st century, including Mexico, the Mediterranean, Southwest Asia, and China. Notably, this occurs without any further expansion or intensification of irrigation beyond current levels, even while greenhouse gas forcing steadily increases. However, the magnitude and significance of these moderating irrigation effects vary across regions and are highly sensitive to the background climate state and the degree to which evapotranspiration is supply (moisture) versus demand (energy) limited. Further, limitations on water and land availability may restrict our ability to maintain modern irrigation rates into the future. Nevertheless, it is likely that irrigation, alongside other components of intensive land management, will continue to strongly modulate regional climate impacts in the future. Irrigation should therefore be considered in conjunction with other key regional anthropogenic forcings (e.g., land cover change and aerosols) when investigating the local manifestation of global climate drivers (e.g., greenhouse gases) in model projections.

Plain Language Summary Alongside increasing global greenhouse gas concentrations, climate is also sensitive to regional climate forcings, including changes in land use and land management. During the twentieth century, the expansion and intensification of irrigation strongly diminished warming trends in many regions. Here, we demonstrate that maintaining modern irrigation rates into the future would continue to modulate regional warming and soil moisture drying during the 21st century, even as greenhouse gas forcing continues to increase. However, the magnitude of these irrigation effects is highly sensitive to regional climate differences, and critical limitations on water and land availability may limit our ability to continue irrigation rates at modern levels.

1. Introduction

Irrigation is the single largest category of human water use, accounting for 60–70% of global freshwater withdrawals and up to 80% of consumption (Siebert et al., 2015; Wada et al., 2013). Beyond the well-established importance of irrigation for agricultural production (Siebert et al., 2005, 2015), the effects of irrigation on the climate system itself are also being increasingly recognized. Empirical and modeling studies have demonstrated how irrigation can reduce surface and air temperatures (Chen & Dirmeyer, 2019; Cook et al., 2015; Kueppers et al., 2007; Nocco et al., 2019; Puma & Cook, 2010; Singh et al., 2018), diminish heat extremes (Lobell et al., 2008; Thiery et al., 2017, 2020), and increase precipitation (DeAngelis et al., 2010; Lo & Famiglietti, 2013; Yang et al., 2017). There is even strong evidence that irrigation-induced cooling has reduced the magnitude of greenhouse gas-forced warming trends in some regions (Bonfils & Lobell, 2007; Lobell & Bonfils, 2008; Lobell et al., 2008; Nocco et al., 2019). These effects can be so large that intensive land management, including irrigation, has even been proposed as a potential strategy for ameliorating the regional and local effects of global warming (Hirsch et al., 2017; Seneviratne et al., 2018).

There are, however, outstanding uncertainties regarding the role of irrigation in historical and future climate evolution, especially alongside other anthropogenic forcings. Notably, while irrigation (and its effect on

climate) expanded and intensified rapidly over the twentieth century (Siebert et al., 2015), this expansion has slowed considerably in recent years (Wada et al., 2013). In fact, most irrigation scenarios for the future indicate it is unlikely that irrigation will increase substantially, if at all, in the coming decades, a consequence of climate change and declining land and water resources (Elliott et al., 2014; Faurès et al., 2002; Turral et al., 2011). Furthermore, while some studies have investigated the effects of irrigation under future warming scenarios (Cook et al., 2011), none have considered the potentially time transient nature of the irrigation response should irrigation rates stop expanding or start declining while global forcing (e.g., anthropogenic greenhouse gases) continues increasing. Therefore, while the historical influence of irrigation on climate has been widely investigated, the capacity of irrigation to continue influencing regional climate in the face of ongoing and future increases in greenhouse gas forcing remains an open question.

Here, we investigate the potential for modern irrigation rates to continue influencing regional climate during the 21st century using an existing 20-member ensemble simulation of the GISS climate model ("ModelE") forced by a high warming greenhouse gas scenario (RCP 8.5). While previous analyses using ModelE have focused on the influence of irrigation in the historical period (Cook et al., 2015; Puma & Cook, 2010), or investigated irrigation in the future using simplified equilibrium simulations (Cook et al., 2011), our analyses are centered on the impact of modern irrigation rates alongside rising greenhouse forcing. This allows us to evaluate the potentially transient magnitude and significance of irrigation effects on temperature and soil moisture as global forcing steadily increases, but irrigation remains fixed, for the 21st century. We specifically address two primary research questions: (1) How does summer climate evolve in irrigated regions, relative to adjacent nonirrigated regions? and (2) how does the effect of modern irrigation rates on surface air temperature (SAT) and soil moisture anomalies change with rising greenhouse gas forcing in the 21st century?

2. Materials and Methods

Our study uses the GISS-SST ensemble, a 20-member SST-forced ensemble (at 2° × 2.5° spatial resolution) of the latest version (v2.1) of the GISS climate model, ModelE. GISS-SST was originally developed to investigate how SST forcing of regional hydroclimate would change under enhanced greenhouse gas forcing in the future (Cook et al., 2019), but all GISS-SST ensemble members also include irrigation as an external anthropogenic forcing. Here, we use GISS-SST as an "ensemble of opportunity" to investigate the degree to which modern irrigation will continue to influence climate as greenhouse warming intensifies in the 21st century, using an analysis approach detailed under section 2.3. First, we provide a broad summary of the setup of the GISS-SST ensemble and refer interested readers to Cook et al. (2019) for the complete details.

2.1. The GISS-SST Ensemble

Over the historical period (1871–2014), all 20 GISS-SST ensemble members are identically forced with the HadiSST sea ice and SST data set (Rayner et al., 2003) and CMIP6 historical climate forcings (Eyring et al., 2016). Each individual ensemble member uses a unique set of initial conditions in the atmosphere and land surface (soil temperature and moisture) sampled from a 500-year-long preindustrial simulation that uses fixed 1850 forcings and climatological average HadiSST sea ice and SSTs from the years 1876–1885. Each ensemble member continues running from 2015–2100, using RCP 8.5 forcings and a new SST and sea ice forcing data set. To generate the new SSTs and sea ice, we linearly detrend the HadiSST data sets from 1915–2100, retaining interannual to multidecadal variability but removing any long-term changes in temperature or sea ice concentrations. We then superimpose this variability on 2015–2100 SST and sea ice trends taken from a separate nine-member slab ocean (q-flux) ModelE ensemble simulation using CMIP6 historical (1871–2014) and RCP 8.5 (2015–2100) forcings. With this approach, we generated a new synthetic SST and sea ice data set with variability representative of the historical record from 1915–2000, but with long-term trends (characterized by ocean warming and declining sea ice) consistent with the ModelE response to RCP 8.5 forcings from 2015–2100. All vegetation types in ModelE, including crops and natural vegetation (up to 17 different plant functional types; see Kim et al., 2015, for more details), share soil moisture from the same soil column. While GISS ModelE does not have dynamic vegetation, it includes plant physiological responses (gross primary productivity and stomatal conductance) to atmospheric CO_2 concentrations.

Global warming in GISS-SST, defined as the change in global, annual average SAT anomalies, is ≈5 K above preindustrial by the end of the 21st century (Figure 1a), comparable to the warming in the NCAR Large Ensemble simulation (Kay et al., 2014). While the GISS-SST ensemble uses a high emissions, high warming

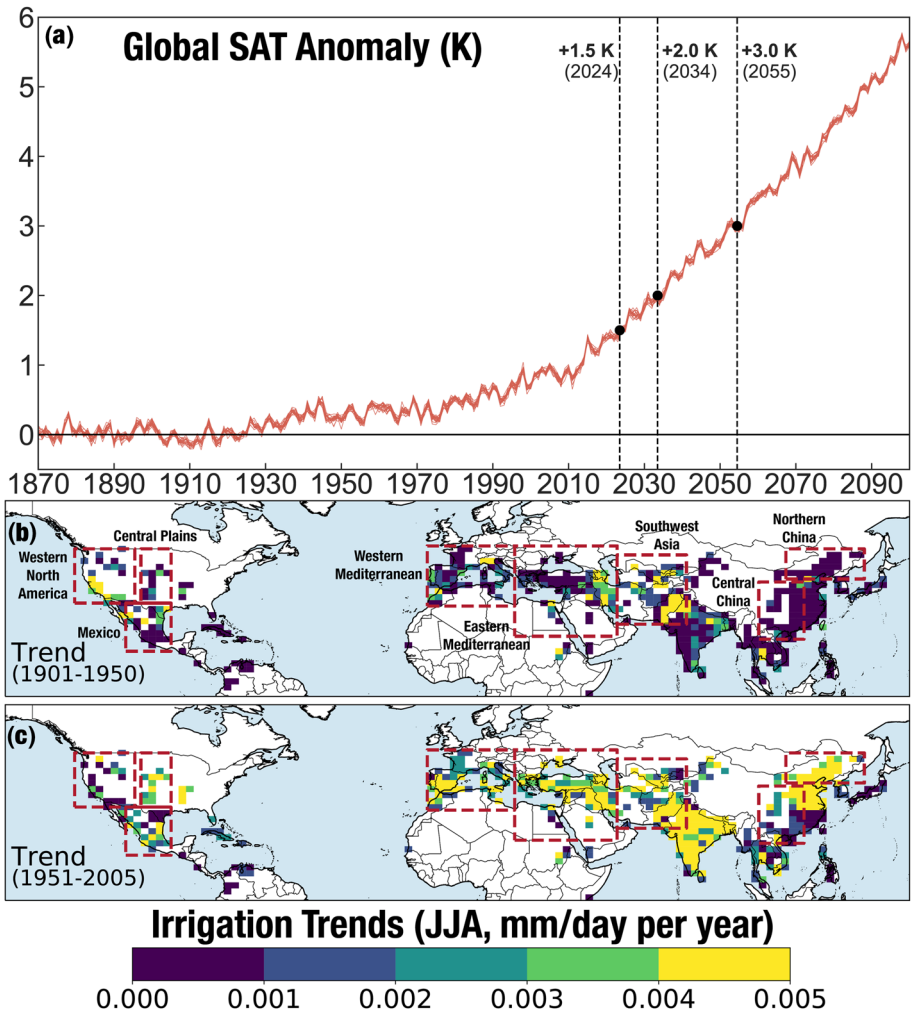

Figure 1. (a) Global annual average surface air temperature (SAT) anomalies (Kelvins) in the GISS-SST ensemble. Each red line is an SAT time series from an individual ensemble member. Vertical dashed lines indicate dates when, in the ensemble average, SAT crosses major warming thresholds: +1.5 K (2024), +2.0 K (2034), and +3.0 K (2055). (b, c) Trends in boreal summer (June-July-August; JJA) irrigation (mm/day/year) for two twentieth century intervals (1901–1950 and 1951–2005) in the data set used to force the GISS-SST ensemble. For the 21st century (2006 to 2100), irrigation is fixed in time, equivalent to rates in 2004. The areas labeled and outlined in red are the main regions of analysis, within which climate is compared between irrigated (IRR) and adjacent, nonirrigated (NON) grid cells.

scenario (RCP 8.5), we emphasize that the intention here is not to present a formal projection or argue that such a simulation represents a "business-as-usual" trajectory for the evolution of the climate system in the near future. Rather, this scenario allows us to evaluate how the effects of irrigation will change across a wide range of warming thresholds as the climate in the ensemble evolves over the 21st century. Some of these thresholds are highlighted in Figure 1a (vertical dashed lines), and in later figures, denoting the dates when SAT warming reaches +1.5 K (2024), +2.0 K (2034), and +3.0 K (2055) above preindustrial.

2.2. Irrigation in GISS ModelE

Irrigation in ModelE is not calculated prognostically but is instead prescribed as a time-varying forcing based on an updated version of the offline calculated irrigation water demand (IWD) data set of Wisser et al. (2010), which includes provisioning for paddy production and inefficiencies (Wada et al., 2014; Wisser et al., 2010). This IWD data set is generated by combining the University of Frankfurt/FAO Global Maps of Irrigated Areas (Siebert, Döll, Feick, & Hoogeveen, 2005; Siebert, Döll, Hoogeveen, et al., 2005), an offline terrestrial water balance model (Federer et al., 2003; Vörösmarty et al., 1998), and crop-specific calendars, growing season lengths, and water demand coefficients that account for regional cropping practices (Portmann et al., 2010; Siebert & Döll, 2010). Over irrigated areas, IWD is then estimated as the water required to ensure

optimal crop growth. The modeling approach described in Wada et al. (2014) is considered to be among the state-of-the-art approaches and is also being used to contribute to ISIMIP activities (Schewe et al., 2014), which are ongoing efforts to use the latest techniques to constrain water resource use globally and regionally.

This IWD data set provides some of the best empirically constrained global estimates of irrigation applications currently available. Importantly, irrigation in the field is not solely constrained by crop water demand but is also influenced by decision making in response to conventional or traditional management practices, market prices, power availability, leakage and abstraction efficiencies, farmer behavior, and other pressures or incentives that extend beyond crop and environmental water losses (Grogan et al., 2017; Levidow et al., 2014; Nazemi & Wheater, 2015). These can be all the more influential than climatic water demand in heavily irrigated regions, especially those that rely on groundwater and use it in unsustainable ways (Bassi, 2014; Grogan et al., 2017; Rodell et al., 2009). The estimates we use in ModelE from the offline modeling approach attempt to account for some of these nonbiophysical influences on applied irrigation water, for example, by using empirical data sets of irrigated areas and crop calendars to constrain the seasonal timing, spatial extent, and trends in irrigation intensity and extent. This data set thus serves to capture irrigation as a human forcing, rather than one constrained by crop water demand alone.

Within ModelE, this estimated IWD is applied as a forcing to the vegetated portion of the grid cell below the vegetation canopy where, for days with irrigation rates above zero, irrigation is applied at every model time step and is distributed evenly throughout the day. Initially, water to satisfy the irrigation demand is sourced from surface reservoirs (lakes and rivers) within the same irrigated grid cell. If, however, this flux is insufficient to fully satisfy the prescribed IWD, additional water is added from outside of the system, conceptually representing fossil groundwater. As in the real world, where fossil groundwater is disconnected from the hydrological cycle in the modern climate system, this additional flux of water for irrigation represents an addition to the total mass of water within ModelE. Despite its simplified representation, irrigation in ModelE has been used successfully to investigate historical and modern irrigation impacts on climate (Cook et al., 2015; Puma & Cook, 2010; Singh et al., 2018). Additionally, previous work has demonstrated that inclusion of irrigation in ModelE improves the simulated variability of summer monsoon circulation indices over South Asia (Shukla et al., 2014).

In the GISS-SST ensemble, irrigation from 1901–2015 is prescribed according to the historically varying data set of Wisser et al. (2010). Over the late nineteenth century (1871–1900), during which empirical IWD estimates are not available, irrigation is estimated by linearly interpolating early twentieth century irrigation rates back in time. From 2006–2100, irrigation is fixed in time (set to the irrigation rate for 2004 every year), effectively representing a future irrigation scenario where current irrigation levels are maintained. Irrigation rates have increased steadily over the historical period, accelerating in many regions from the early (1901–1950) (Figure 1b) to late (1951–2005) (Figure 1c) twentieth century. Irrigation is highly localized in some of the most agriculturally productive regions of the world (e.g., the Central United States, India, and China), but at the hemispheric and global scale, the most widespread and highest irrigation rates are in monsoon Asia.

Historical changes in irrigation over our eight regions of interest (Figure 2) are in line with broader hemispheric irrigation trends toward increased irrigation rates. In all regions, irrigation increases over the twentieth century, with a notable acceleration after 1950 in some areas, especially the Central Plains, Central China, and Northern China. Irrigation rates are generally higher over the regions in Asia, especially in Southwest Asia.

2.3. Analyses

We focus on irrigation effects on climate during the boreal summer (JJA) in the Northern Hemisphere. Climate responses to irrigation are likely to be largest during the summer, which is the time of year in most regions when evaporative demand is highest, land-atmosphere coupling is strongest, and irrigation reaches its peak annual levels. We acknowledge, however, that irrigation rates outside of these months can be high (e.g., the dry premonsoon season over India) and irrigation impacts in these seasons may be different compared to JJA. We also focus on two variables: SAT and near-surface soil moisture from the top two layers, extending to a depth of approximately 30 cm. While other variables are also likely sensitive to irrigation (e.g., humidity), SAT and soil moisture have direct relevance for impacts and will be directly responsive to irrigation. Further, we expect that because of the local nature of the response of these variables to irrigation, these will be relatively straightforward to assess using the analysis approach we have outlined below.

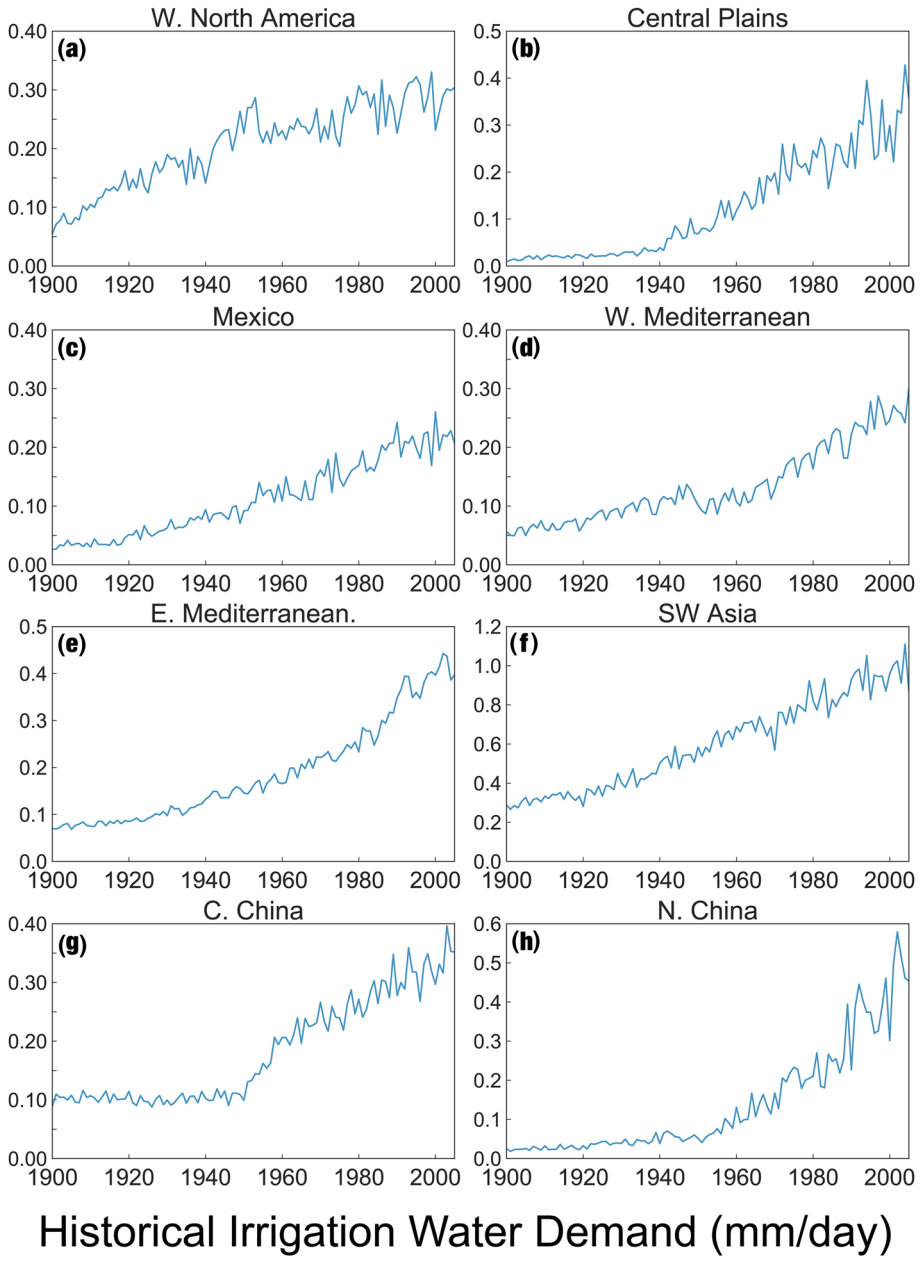

Figure 2. Over our eight regions of interest, area average boreal summer (June-July-August; JJA) irrigation rates (mm/day) from 1900–2005. These rates are taken from the data set of Wisser et al. (2010) and then applied as a forcing to the land surface in ModelE.

Ideally, we would be able to compare the climate response over irrigated grid cells in the GISS-SST ensemble with an alternative, counterfactual ensemble simulation that excludes irrigation. However, the computational cost (approximately 400,000–500,000 processor hours) of generating a new version of the GISS-SST ensemble without irrigation is prohibitively expensive with our current computational resources. Therefore, we instead compare anomalies and trends in SAT and soil moisture between irrigated (defined as grid cells with modern, annual average irrigation rates ≥0.05 mm/day; IRR) and adjacent, nonirrigated (defined as cells with modern annual average irrigation rates <0.05 mm/day; NON) grid cells within the ensemble. The NON grid cells include cells that are diagonally adjacent to IRR grid cells. For analysis purposes, both the IRR and NON grid cells are fixed in time using this criteria, including over both the historical and future time intervals.

Our methodology is similar to previous studies that use a proximity based, moving search window to identify climate impacts from local forcings, including irrigation and land use change (Chen & Dirmeyer, 2019; Kumar et al., 2013; Lejeune et al., 2017). However, because of the coarse spatial resolution of ModelE (which limits the number of grid cells available for sampling), we do not compare individual irrigated grid cell responses. Instead, we select several large regions (outlined in Figure 1 and detailed in the next paragraph), which include broadly even sampling of IRR and NON grid cells. Specifically, the ratio of IRR to IRR + NON cells in all of our regions falls between 0.35 and 0.65, consistent with the sampling criteria used in Chen and Dirmeyer (2019). Within each region, we average climate responses over the IRR grid cells and NON grid cells separately and then compare the two to assess the irrigation response. As with the studies cited above that use a similar approach, the implicit assumption is that neighboring grid cells should have similar responses to global-scale forcing changes (e.g., anthropogenic greenhouse gases) and will be primarily differentiated by the local forcing differences (in our case, irrigation). For some regions, our analysis approach may underestimate the spatial extent of irrigation impacts because we focus solely on the effects of irrigation on temperature and soil moisture within irrigated grid cells. Numerous studies, however, have documented how the influence of irrigation can extend remotely over broad regions as a consequence of heat and moisture transport by the atmosphere (DeAngelis et al., 2010; de Vrese et al., 2016; Lo & Famiglietti, 2013).

The main regions we focus on are outlined in the dashed red boxes in Figure 1, representing areas with mixes of irrigated and nonirrigated grid cells across a diversity of climate regions. Because of the sampling constraint that each of our regions must include a mix of IRR and NON grid cells, we were forced to exclude some of the most heavily irrigated regions, including peninsular India and coastal China. The regions we chose were as follows: Western North America (127°W–107°W, 31°N–49°N; ratio of IRR to IRR + NON grid cells = 0.36), the Central Plains (105°W–95°W, 31°N–49°N; ratio = 0.39), Mexico (110°W–95°W, 15°N–31°N; ratio = 0.64), Western Mediterranean (10°W–19°E, 30°N–50°N; ratio = 0.62), Eastern Mediterranean (19°E–53°E, 20°N–50°N; ratio = 0.52), Southwest Asia (53°E–76°E, 24°N–47°N; ratio = 0.53), Central China (100°E–115°E, 19°N–38°N; ratio = 0.63), and Northern China (109°E–135°E, 39°N–49°N; ratio = 0.52).

In some regions, there may be substantial differences in climate between the IRR and NON grid cells that are unrelated to irrigation. For example, over Western North America, many of the adjacent, nonirrigated grid cells occupy higher elevation areas that are likely to have higher absolute precipitation during the summer relative to lower elevations, where most of the irrigation occurs. We note, however, that our determination of whether irrigation continues to have climate impacts in the future is primarily focused on comparisons of trends and anomalies (i.e., "Are nonirrigated regions warming or drying more over time than adjacent irrigated areas?"), rather than absolute differences. While imperfect, in the absence of alternative simulations excluding irrigation, this comparison is therefore the most appropriate for estimating the climate impact of irrigation in this ensemble. For regions where there are apparent differences in climate between IRR and NON that appear unrelated to irrigation, we discuss this and use this information to contextualize our assessment of irrigation effects on climate.

3. Results

3.1. Climate Trends in Irrigated and Adjacent Regions

Warming (Figure 3) dominates across most regions over both IRR and NON grid cells, especially after 2006. For many areas (e.g., Mexico, Central Plains, China, and the Mediterranean), warming trends are larger during the early (1901–1950) compared to late (1951–2005) twentieth century, despite the increase in greenhouse gases and other anthropogenic forcings over time. These time-varying warming trends over the twentieth century may reflect, in part, the strong cooling effect from rapidly expanding and intensifying irrigation rates over some regions during the latter period (Figures 1 and 2). However, other forcing agents are also changing over time (e.g., land cover and aerosols), as are other variables (e.g., precipitation) relevant for SAT, precluding a formal attribution analysis with the existing simulations. As greenhouse gas forcing rapidly increases in the 21st century, and irrigation is held constant at the current rates, much more widespread and intense warming appears nearly everywhere.

Precipitation trends are more spatially heterogeneous than the SAT trends (Figure 4). The largest model response is over peninsular India, which shows strong wetting from 1901–1950, followed by drying from

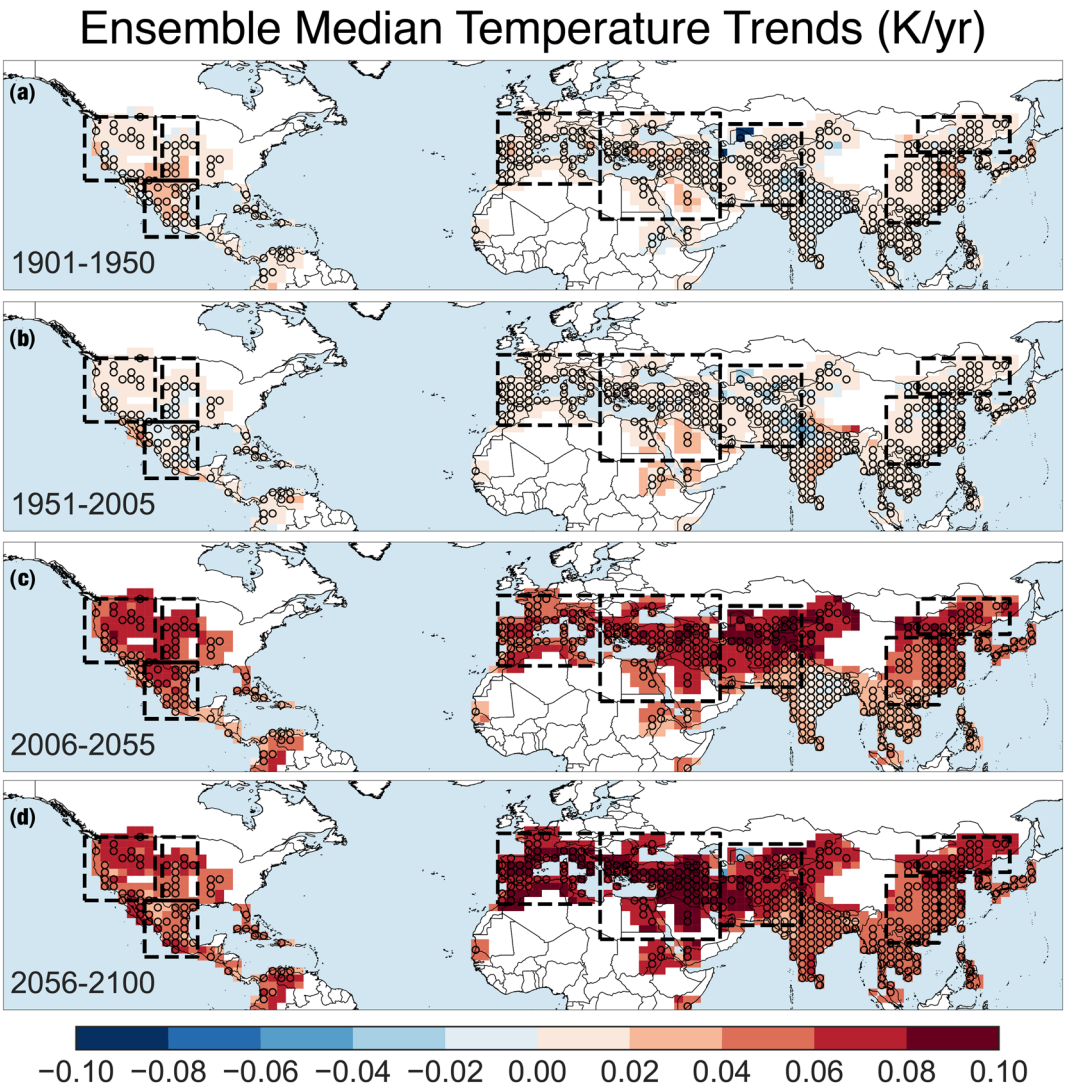

Figure 3. Ensemble median boreal summer (JJA) SAT trends (K/year) for irrigated (IRR; indicated by open circles) and adjacent, nonirrigated (NON) grid cells in the GISS-SST ensemble. As noted in the text, NON grid cells include those that are diagonally adjacent to the IRR grid cells. Trends are calculated within each ensemble member first, and then the median of these trends is calculated and shown in the figure. Dashed black boxes indicate the regions within which IRR and NON grid cells are separately averaged and compared in later analyses.

1951–2005, and a stronger wetting trend from 2006–2055. The late twentieth century drying is broadly consistent with other model analyses of irrigation and the monsoon, which show that irrigation weakens the monsoon by altering land-ocean temperature contrasts (Guimberteau et al., 2012; Shukla et al., 2014; Singh et al., 2018). The precipitation trends track closely with the SAT trends over India and may be the primary driver of temperature trends over this region: strong warming and precipitation drying from 1951–2005 and weak SAT trends and increasing precipitation from 1901–1950 and 2006–2055. As with SAT, however, changes in other forcings within the simulations mean that these shifts in the monsoon cannot be explicitly attributed to any single factor.

Near-surface soil moisture trends reflect changes in precipitation, evaporative losses, and (where applicable) irrigation (Figure 5). In most irrigated grid cells, trends during the twentieth century are toward wetter soils, especially over the Mediterranean, northwest India, Northern China, and Southwest Asia. Northwest India represents one of the most intensely irrigated regions in our ensemble, and the pronounced soil moisture wetting here may explain the intense cooling in this region during 1951–2005 (Figure 2). This contrasts with the rest of India where soil moisture dries (Figure 5), consistent with declining precipitation (Figure 4). From

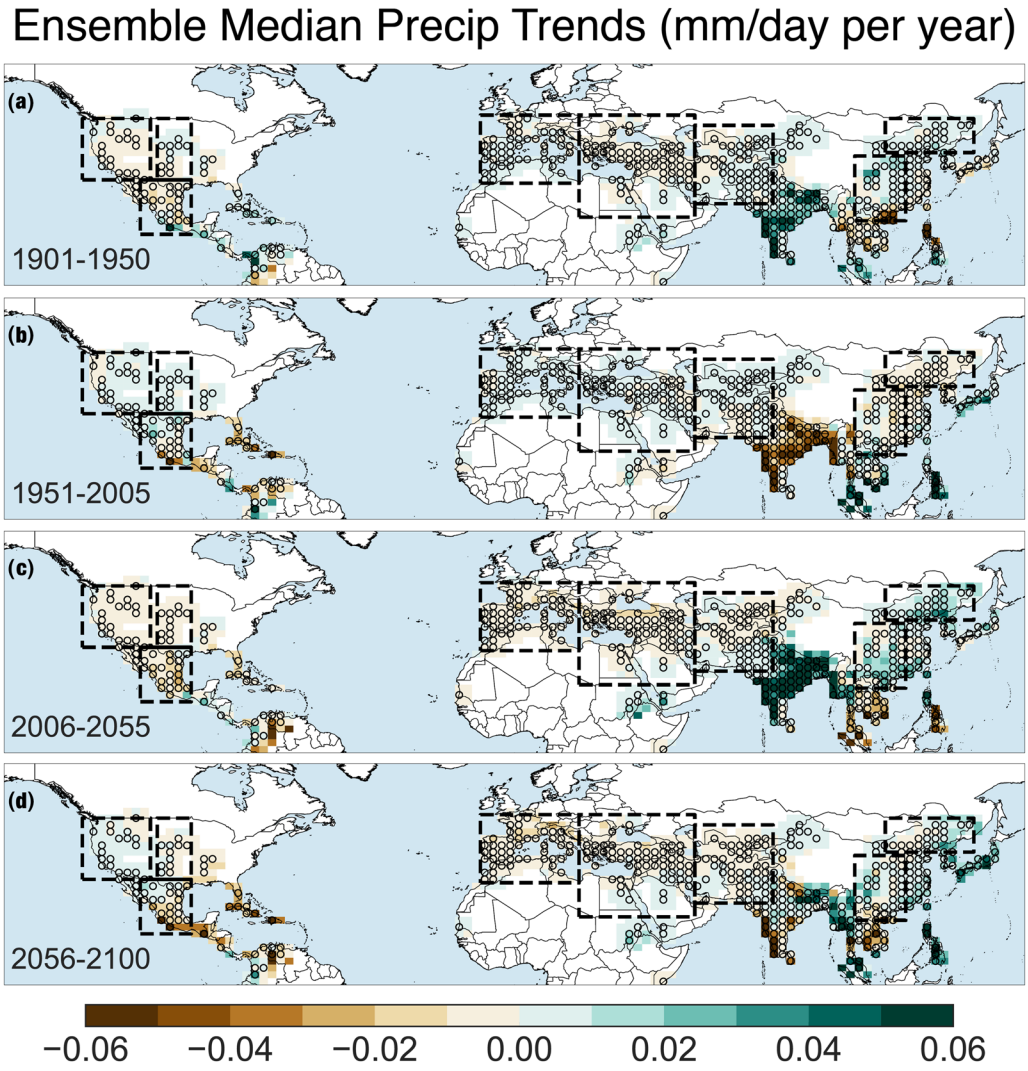

Figure 4. Ensemble median boreal summer (JJA) precipitation trends (mm/day/year) for irrigated (IRR; indicated by open circles) and adjacent, nonirrigated (NON) grid cells in the GISS-SST ensemble. Trends are calculated within each ensemble member first, and then the median of these trends is calculated and shown in the figure. Dashed black boxes indicate the regions within which IRR and NON grid cells are separately averaged and compared in later analyses.

2006–2055, wetting continues over peninsular India, despite the fact that irrigation is stable in time, and may be a consequence of large increases in precipitation. For 2056–2100, precipitation no longer increases over India and soil moisture declines as warming continues. Outside of this region, soil moisture trends throughout irrigated areas in the 21st century are mostly toward drying.

Median zonal trends in SAT and soil moisture for IRR and NON grid cells are compared in Figure 6. SAT trends across latitudes are uniformly positive (warming) for all four time intervals (Figures 6a–6d), a direct response to the steadily increasing greenhouse gas forcing. For most latitudes and time periods, however, warming trends are significantly (two-sided Wilcoxon rank-sum test, $p \leq 0.05$, $n = 20$) lower in IRR versus NON, indicating that irrigation is moderating the warming. This effect is especially pronounced from 1951–2005, when irrigation increases rapidly and significantly slows the warming across most latitudes from 10°N–30°N. Notably, this cooling forcing from irrigation (i.e., reduced warming trends over IRR versus NON) continues into the 21st century across most latitudes, despite the fact that irrigation is no longer increasing.

Irrigation impacts on zonal soil moisture trends (Figures 6e–6h) are more variable in space and time, likely because of the sensitivity of soil moisture to a host of variables (e.g., precipitation) that will not respond as

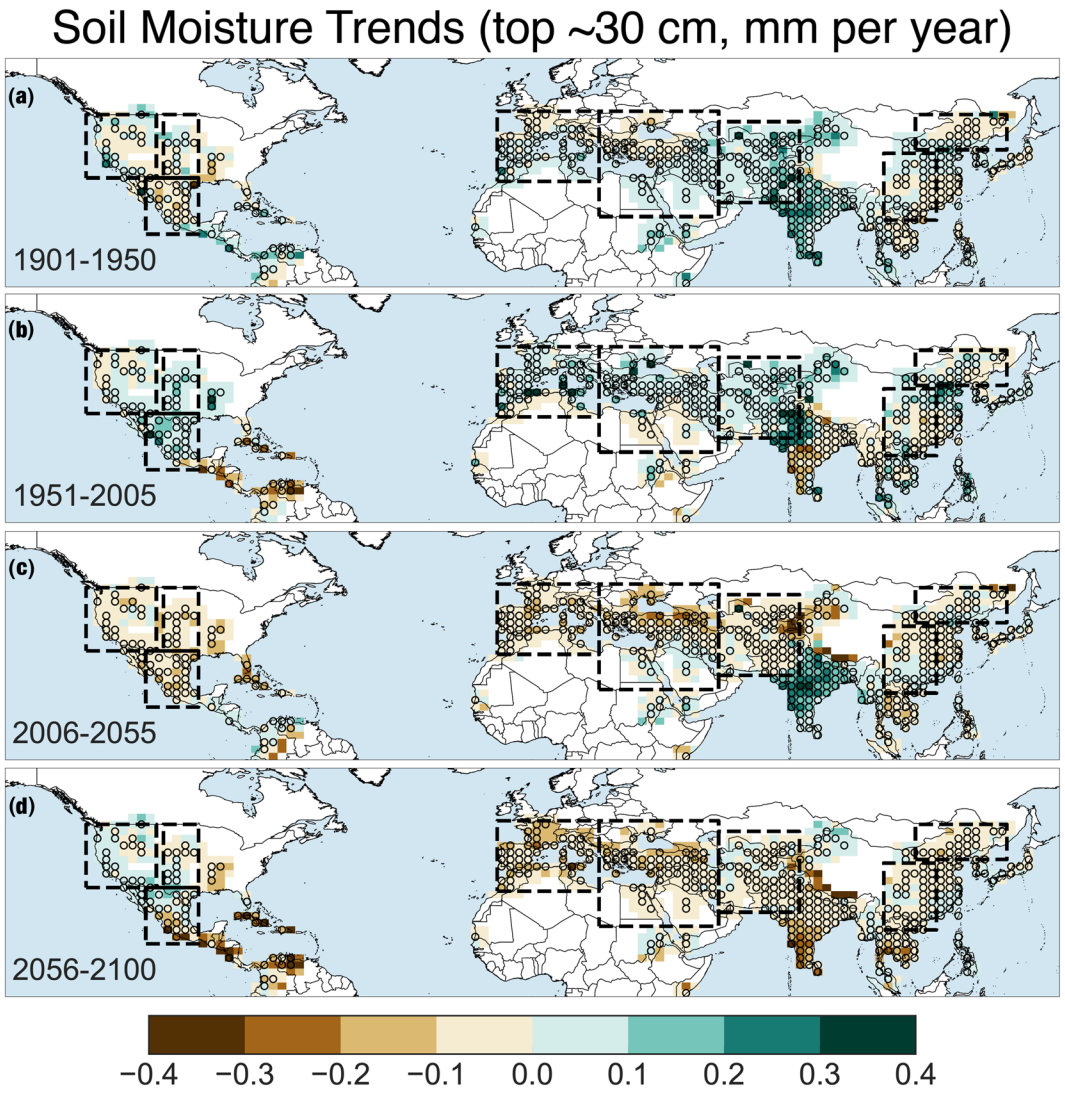

Figure 5. Ensemble median boreal summer (JJA) trends (mm/year) in near surface (surface to a depth of ≈30 cm) soil moisture for irrigated (IRR; indicated by open circles) and adjacent, nonirrigated (NON) grid cells in the GISS-SST ensemble. Trends are calculated within each ensemble member first, and then the median of these trends is calculated and shown in the figure. Dashed black boxes indicate the regions within which IRR and NON grid cells are separately averaged and compared in later analyses.

uniformly or homogeneously as temperature. Soil moisture trends are mostly positive or near zero during the twentieth century, and there is a clear irrigation effect in most latitudes to either diminish drying or amplify wetting trends. During the twentieth century, the largest trends (positive and negative) occur at latitudes below 10°N and may reflect sampling issues at these latitudes. For example, the spatial extent of irrigation is greatest between 20°N and 45°N, with the number of IRR and NON grid cells typically ≥20 for any latitude band at these latitudes. By contrast, fewer than 10 (and in some cases, <5) IRR or NON grid cells are available at any given latitude between 0°N and 10°N, and (because of the large ocean area) these cells are sparsely sampled across disparate regions. Over the 21st century, soil moisture trends are mostly toward drying, especially in the midlatitudes above 30°N in 2006–2055 and across all latitudes from 2056–2100. Irrigation effects are more mixed during these periods, with the most significant impacts manifesting in 2006–2055 between 15°N and 30°N.

3.2. Coherency of Climate Trends and Variability Across IRR and NON Grid Cells

As with previous studies using a similar analysis approach (Chen & Dirmeyer, 2019; Kumar et al., 2013; Lejeune et al., 2017), we implicitly assume analogous responses to global forcing and large-scale climate

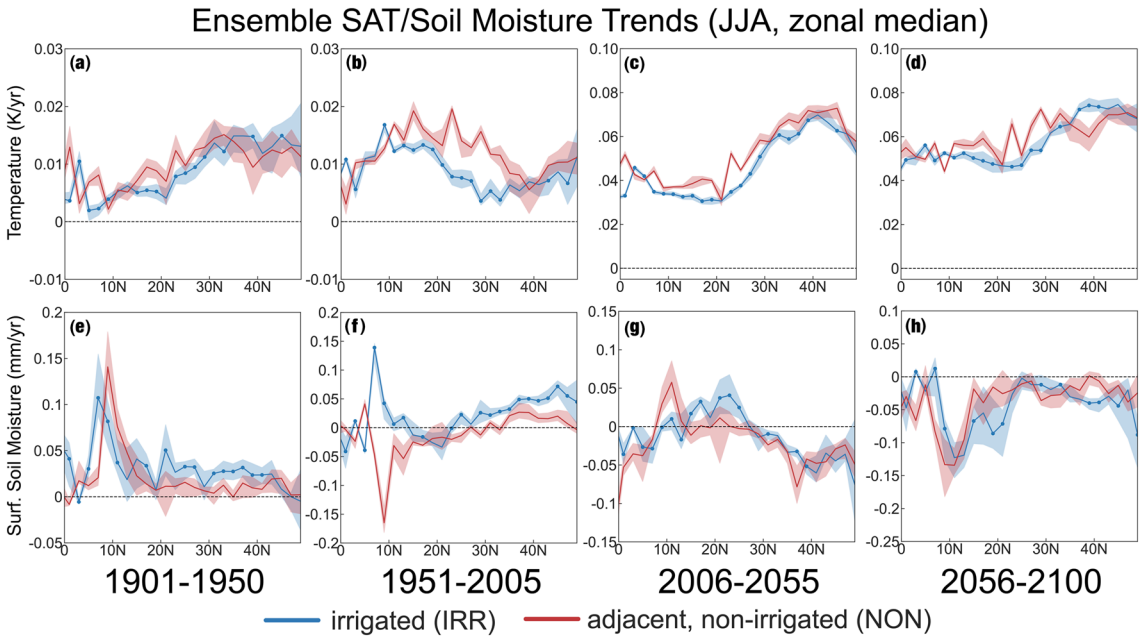

Figure 6. (a–h) Median zonal SAT (K/year) and soil moisture (mm/year) trends for irrigated (IRR) and adjacent, nonirrigated (NON) grid cells in the GISS-SST ensemble over our four periods of analysis. Solid lines indicate the ensemble median; shading indicates the 25th–75th percentile range across the ensemble. Solid dots indicate latitudes where the ensemble median trend is significantly different (two-sided Wilcoxon rank-sum test, $p \leq 0.05$, $n = 20$) between IRR and NON.

variability over IRR and NON grid cells, such that differences between the two can be primarily attributed to irrigation. To test this assumption, we compare the long-term JJA temperature evolution and variability between IRR and NON grid cells within each of our regions (Figure 7). Changes over time in the long-term warming trends are similar between IRR and NON in all regions, even as irrigation acts to substantially reduce much of the total warming in the late 20th and 21st centuries for some regions. For example, both IRR and NON grid cells show modest early twentieth century warming, a slowdown in warming during the midtwentieth century, and accelerated warming after the 1970s and out to 2100. Interannual variability is also strongly coherent between IRR and NON, which we demonstrate by calculating Pearson's correlations between the IRR and NON time series within each region after first differencing the time series to remove long-term changes and low-frequency variability. The median correlations, calculated across all 20 ensemble members, are shown in the lower right corners of each panel in Figure 7. For most regions, these correlations are in excess of 0.90, with the weakest magnitude over the Western Mediterranean (though still >0.70). From these analyses, we conclude that global climate forcings and large-scale climate variability in each of our regions are evenly expressed across IRR and NON grid cells, satisfying our initial assumptions that these grid cells can be primarily differentiated in terms of the effects of irrigation.

3.3. Surface Air Temperature and Soil Moisture Responses to Irrigation

To evaluate the magnitude and significance of irrigation effects in each region, we calculate differences (IRR minus NON) in summer (JJA) SAT (Figure 8) and soil moisture (Figure 9) *anomalies* (calculated relative to a baseline climatology of 1891–1920) in our eight regions. Colored, vertical lines in both figures indicate the years when global warming in the GISS-SST ensemble passes the +1.5 K (2024), +2.0 K (2034), and +3.0 K (2055) thresholds. Anomalies from the IRR and NON grid cells are averaged together separately, before differences are calculated. These figures therefore show differences in the *changes in SAT and soil moisture* anomalies between IRR and NON, rather than differences in the absolute values. *Negative differences in SAT indicate that warming is reduced* over IRR grid cells compared to NON, while *positive soil moisture differences indicate less drying or more wetting* over IRR versus NON. Years with statistically significant differences between IRR and NON anomalies are indicated by the black dots (two-sided Wilcoxon rank-sum test, $p \leq 0.05$, $n = 20$).

Irrigation reduces greenhouse gas-forced warming in ModelE, though the magnitude, significance, and persistence of this effect vary strongly across our eight regions (Figure 8). Central China, Southwest Asia, the

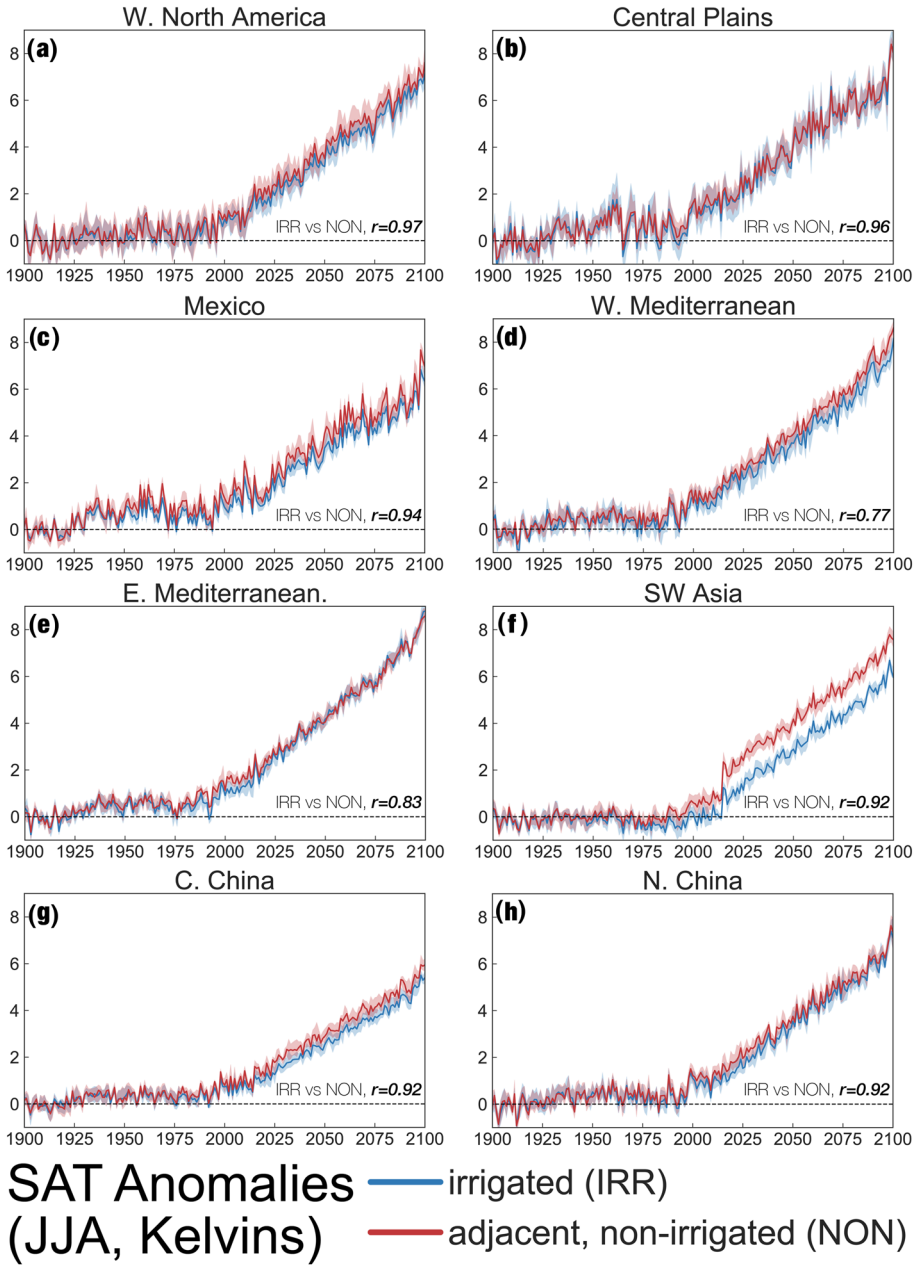

Figure 7. Summer (JJA) surface air temperature anomalies (baseline 1891–1920) for irrigated (IRR) and adjacent, nonirrigated (NON) grid cells for our eight regions of interest. Shading indicates the 25th–75th percentile range across the ensemble. Numbers in the bottom right corners of each panel are the ensemble median Pearson's correlation coefficients, calculated for 1871–2100 after first differencing the IRR and NON time series in each ensemble member.

Western Mediterranean, and Mexico are all regions where significant irrigation cooling effects persist out to the end of the 21st century. For the Eastern Mediterranean and Northern China, however, the effect of irrigation is transient, with strong cooling effects only appearing briefly around the end of the twentieth century and beginning of the 21st century. Twenty-first century irrigation cooling also occurs in Western North America, although the effect is insignificant in most years and is largely absent in the Central Plains. Except for Mexico and Central China, irrigation causes positive and sustained increases in soil moisture, resulting in relative wetting (i.e., greater wetting or reduced drying) over IRR grid cells compared to NON (Figure 9). For most regions, the most significant soil moisture impacts begin in the late twentieth century, reflecting the rapid intensification of irrigation during this period. As with SAT, irrigation effects on soil moisture sta-

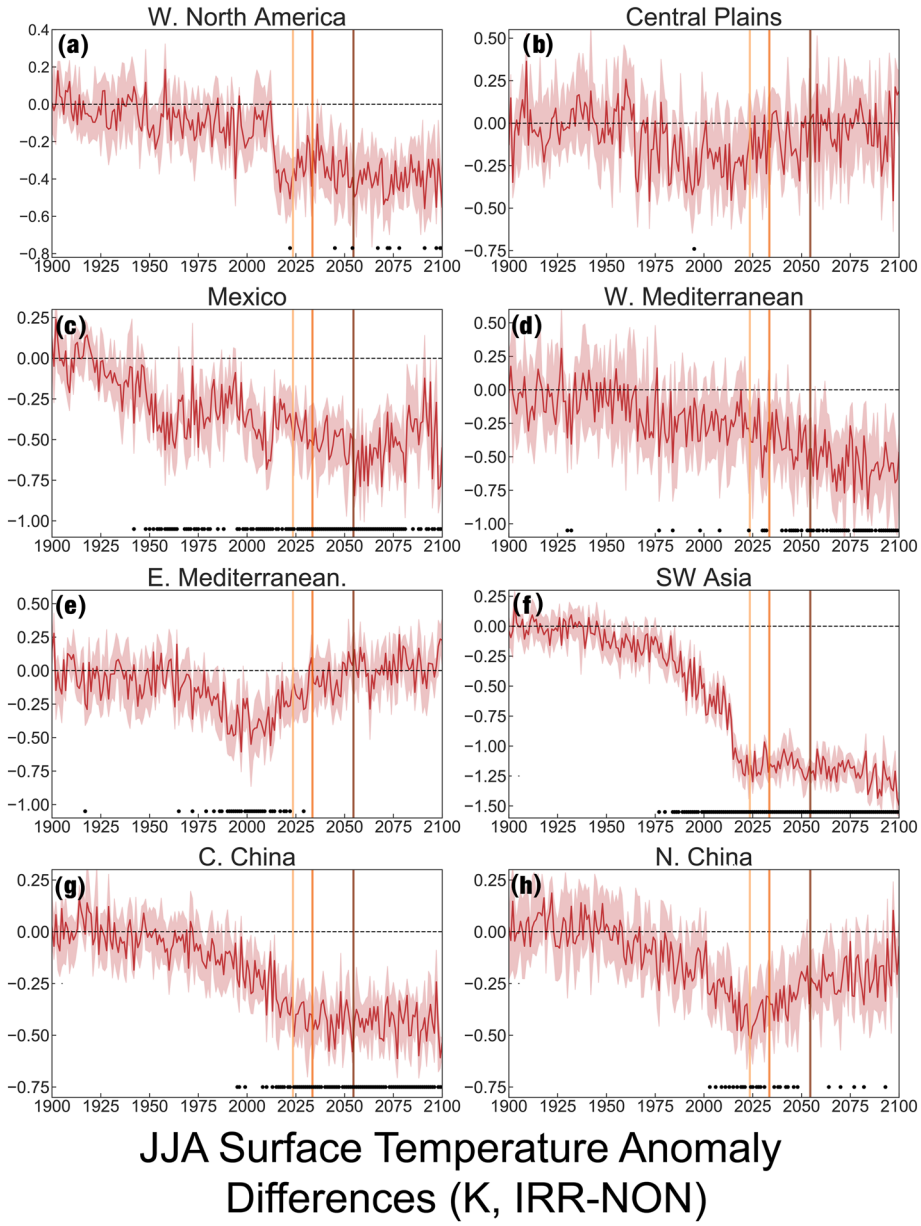

Figure 8. (a–h) Summer (JJA) differences in SAT *anomalies* (baseline 1891–1920) between irrigated (IRR) and adjacent, nonirrigated (NON) grid cells for eight regions. Shading indicates the 25th–75th percentile range across the ensemble. Vertical colored lines indicate dates when, in the ensemble average, SAT crosses major warming thresholds: +1.5 K (2024), +2.0 K (2034), and +3.0 K (2055). Negative differences indicate a reduced magnitude of warming over IRR compared to NON grid cells. Solid dots indicate years where the ensemble median anomalies are significantly different between IRR and NON (two-sided Wilcoxon rank-sum test, $p \leq 0.05$, $n = 20$).

bilize and are sustained to the end of the 21st century in most regions, though they weaken somewhat in the Western Mediterranean.

Quantitative, like-for-like comparisons of irrigation effects on temperature between models and observations, or even across models, are challenging for a variety of reasons. These include the typically much coarser spatial resolution of models compared to observations; the absence of detailed information on actual irrigation amounts and practices in many regions; and irrigation and crop management practices in observations and models, which vary from place to place and are often driven by social and political processes not represented within climate models. The sign of irrigation-temperature responses (i.e., cooling) in ModelE in the regions we investigated is consistent with observations (Chen & Dirmeyer, 2019), including over

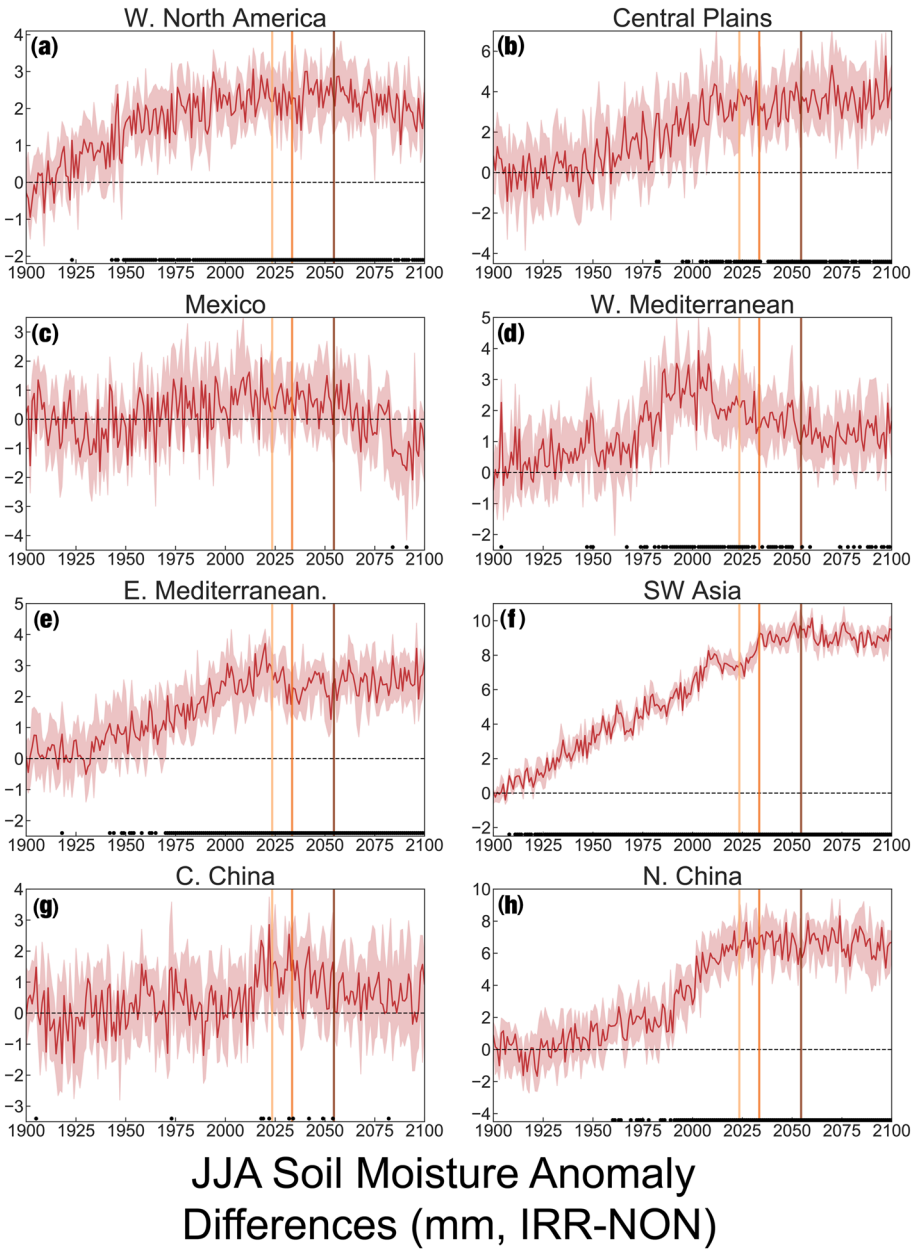

Figure 9. (a–h) Summer (JJA) differences in soil moisture *anomalies* (baseline 1891–1920) between irrigated (IRR) and adjacent, nonirrigated (NON) grid cells for eight regions. Shading indicates the 25th–75th percentile range across the ensemble. Vertical colored lines indicate dates when, in the ensemble average, SAT crosses major warming thresholds: +1.5 K (2024), +2.0 K (2034), and +3.0 K (2055). Positive differences indicate reduced drying, or increased wetting, over IRR compared to NON grid cells. Solid dots indicate years where the ensemble median is significantly different between IRR and NON (two-sided Wilcoxon rank-sum test, $p \leq 0.05$, $n = 20$).

North America (Bonfils & Lobell, 2007; Mahmood et al., 2006, 2013) and China (Han & Yang, 2013; Lobell et al., 2008; Yang et al., 2020) where some of the most detailed empirical analyses of irrigation and climate have been conducted. Many of these same studies also show that this cooling effect is amplified after 1950 as irrigation began rapidly expanding and intensifying (Mahmood et al., 2006), a change that is also apparent in the ModelE temperature responses to irrigation (Figure 8).

Estimates of irrigation cooling effects vary across models and observations in our regions of interest. Yang et al. (2020) estimated irrigation effects on temperature using satellite observations and a similar analysis approach to our study, comparing irrigated areas against nearby nonirrigated regions. For humid areas

of eastern China, where our Northern and Central China regions occur, they estimated a mean irrigation cooling of −0.69 K in daytime land surface temperatures during 2003–2012. Over the same period in ModelE, mean irrigation cooling in SAT was −0.23 K in Central China (Figure 8g) and −0.28 K in Northern China (Figure 8h). Chen and Dirmeyer (2019) used a similar comparison approach across the full Northern Hemisphere from 2002–2017. Over the Great Plains, they documented irrigation-induced cooling of around −1.75 K, while ModelE shows a lesser cooling of only −0.24 K over our Central Plains regions during the same period (Figure 8b). Similarly, Chen and Dirmeyer (2019) show a cooling of around −1 K in observations over eastern China, while in ModelE, the regional irrigation cooling in Central China is only −0.26 K (Figure 8g). Notably, Chen and Dirmeyer (2019) demonstrate that the coupled climate model CESM similarly underpredicts the magnitude of irrigation cooling compared to observations over many regions, though not to the same degree as ModelE. They also show that this underprediction is largest in the lowest spatial resolution version of CESM, which is also approximately the same resolution as ModelE. However, Thiery et al. (2020) found that CESM overpredicts the cooling effect of irrigation on heat extremes.

While these results suggest that ModelE may be underpredicting the cooling effect of irrigation on boreal summer temperature, it is difficult to definitively attribute differences in the irrigation responses between ModelE and observations, or even ModelE and CESM, given the poor observational constraints and challenges inherent in conducting these comparisons. These results do, however, confirm that the sign of temperature responses to irrigation in ModelE is consistent with the available model and observational evidence for irrigation cooling over the historical period.

3.4. Regional Differences in Irrigation Climate Impacts

Irrigation effects on SAT and soil moisture are not spatially uniform (Figures 8 and 9) and may be absent (i.e., SAT in the Central Plains), transient in time (i.e., SAT in the Eastern Mediterranean), or persistent out to the end of the 21st century (e.g., soil moisture in Southwest Asia). Interactions between irrigation and climate are strongly modulated by the baseline hydroclimate (Cook et al., 2011; Puma & Cook, 2010), and differences in the magnitude and significance of irrigation effects may be connected to shifts in hydroclimate over time or differences from region to region. To a first order, irrigation is an additional input of water to the surface that may help compensate for declines in precipitation or increases in evapotranspiration, buffering soil moisture losses relative to grid cells without irrigation. If precipitation increases strongly across IRR and NON grid cells in response to warming, however, the relative benefits of irrigation for soil moisture may be increasingly diminished. Conversely, if precipitation declines strongly, then the relative importance of irrigation for maintaining soil moisture will be magnified.

Cooling from irrigation, in turn, occurs primarily through increased evapotranspiration and upward latent heat fluxes (Cook et al., 2011; Puma & Cook, 2010). The magnitude of this effect depends strongly on the degree to which evapotranspiration in a given region is limited by energy (demand) versus moisture (supply) availability (Koster et al., 2009). This is typically quantified using the evaporative fraction metric, defined as the latent heat flux divided by net radiation at the surface, with the energy partitioning further mediated by vegetation responses. Relatively low evaporative fraction values ($\leq$0.6) are typical of moisture-limited regions, where evapotranspiration and temperature will respond strongly to changes in soil moisture (and therefore irrigation). At extremely low evaporative fractions (less than 0.3 or 0.4), however, temperature responses to irrigation may be limited because any additional water added can be quickly evapotranspired away, leaving the full atmospheric demand unfulfilled and the excess energy allocated toward sensible heating. Conversely, at evaporative fractions greater than 0.6 or 0.7, evapotranspiration is primarily limited by energy availability. For irrigation to affect evapotranspiration and SAT in these regions would therefore typically require some relaxation of existing energy constraints (e.g., increasing evaporative demand by warming the atmosphere).

Here, we characterize the baseline hydroclimate, and changes therein, for each of our regions using *absolute values* of precipitation, near-surface soil moisture, and evaporative fraction. We use this information to interpret the magnitude and significance of the temperature and soil moisture responses to irrigation outlined in Figures 8 and 9.

3.4.1. Western North America and the Central Plains

Over Western North America and the Central Plains, irrigation has a small effect on SAT (Figures 8a and 8b) but a strong and persistent positive effect on soil moisture anomalies (Figures 9a and 9b). Baseline precipitation is higher over NON (red line) versus IRR (blue line) in Western North America, though irrigation brings

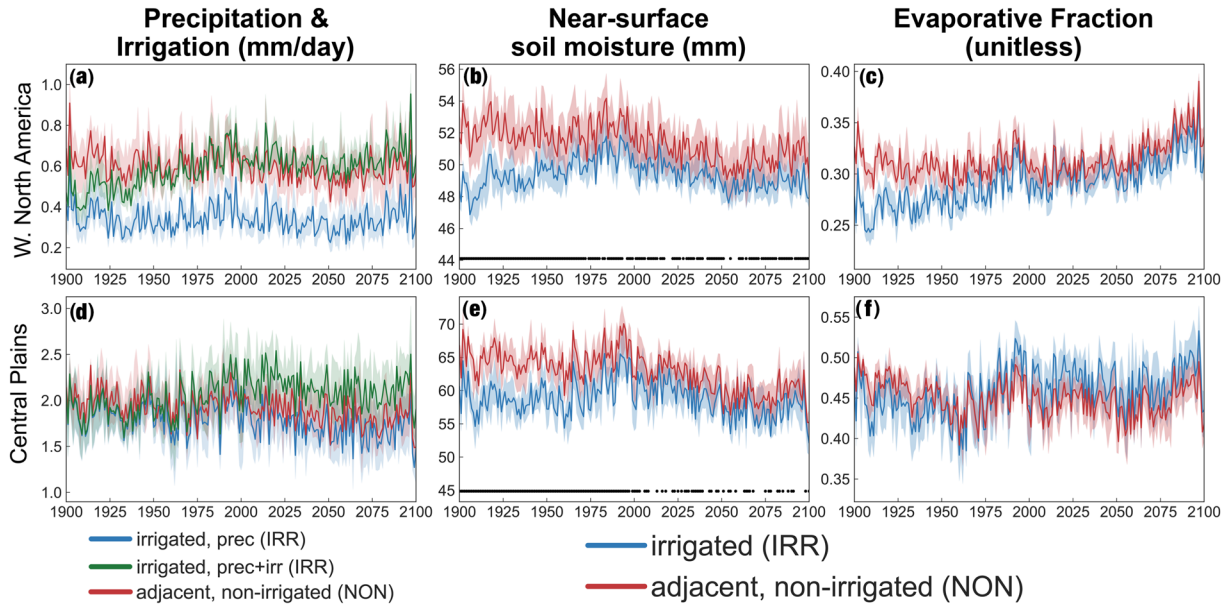

Figure 10. Hydroclimate over IRR (blue and green) and NON (red) grid cells in the GISS-SST ensemble for Western North America (a–c) and the Central Plains (d–f). All variables are expressed in terms of absolute units: precipitation (mm/day; red and blue lines; a, d), precipitation plus irrigation over IRR grid cells (mm/day; green lines; a, d), near-surface soil moisture (mm; b, e), and evaporative fraction (unitless; c, f). Solid lines indicate the ensemble median, while shading shows the 25th–75th percentile range calculated across the ensemble.

total water inputs (green line) in NON and IRR closer to parity (Figure 10a). Absolute soil moisture values are higher over NON (Figure 10b), especially during the twentieth century. Over the Central Plains, total water inputs are similar between IRR and NON during the twentieth century (Figure 10d), with irrigation providing a substantial increase in the 21st century, which helps close the gap in absolute soil moisture between IRR and NON (Figure 10e). As warming accelerates over the 21st century, absolute soil moisture declines in both regions, especially compared to late twentieth century values. Because the NON regions are relatively wetter during the twentieth century, and irrigation during the 21st century causes IRR grid cell water inputs to exceed those in the NON regions, this manifests as a positive soil moisture anomaly difference (Figures 9a and 9b) and a relatively greater drying over NON versus IRR. The lack of a SAT signal from irrigation in both regions likely reflects the modest effect of irrigation on evaporative fraction (Figures 10c and 10f), indicating little change in the surface energy partitioning that is the main driver of irrigation-induced cooling.

3.4.2. Mexico

In contrast to the other North American regions, Mexico shows large and sustained irrigation impacts on SAT anomalies (Figure 8c) but not on soil moisture (Figure 9c). Precipitation and absolute soil moisture decline over both IRR and NON during the 21st century (Figures 11a and 11b). This relatively equivalent drying between both IRR and NON therefore manifests as an insignificant difference in soil moisture trends between IRR and NON and thus a negligible irrigation effect (Figure 9c). However, irrigation does contribute to persistently higher absolute soil moisture values over IRR (Figure 11b), causing a substantial increase in evaporative fraction (+0.10) (Figure 11c). This increase is well within the typical range of values expected for a moisture-limited evaporative regime and is sustained over the entire simulation, indicative of persistently higher latent heating which diminishes warming trends over IRR relative to NON (Figure 8c).

3.4.3. Western and Eastern Mediterranean

Irrigation reduces warming (Figures 8d and 8e) and soil moisture drying (Figures 9d and 9e) in the Western and Eastern Mediterranean, though the SAT effect in the Eastern Mediterranean is transient and significant only around the turn of the 21st century. Both regions experience robust precipitation declines over the IRR and NON grid cells (Figures 12a and 12d), especially during the 21st century, which causes drying in absolute soil moisture (Figures 12b and 12e). In both regions, irrigation is sufficient to at least partially compensate for the declines in precipitation, resulting in reduced relative soil moisture drying over the IRR grid cells (Figures 9d and 9e).

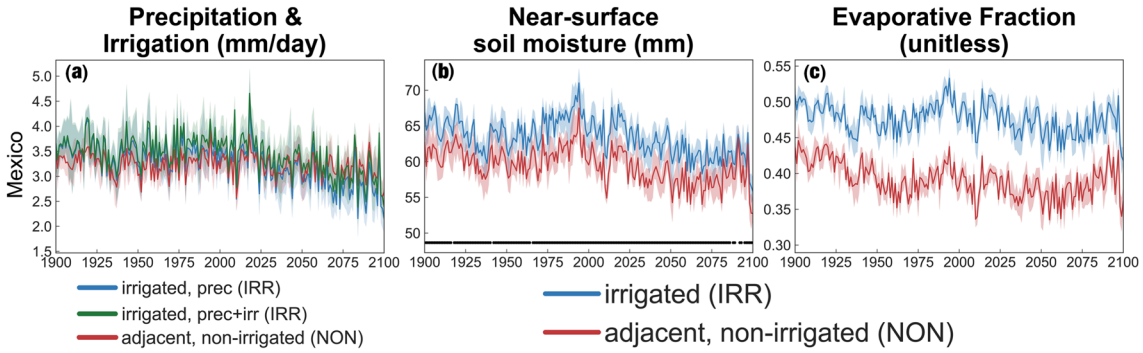

Figure 11. Hydroclimate over IRR (blue and green) and NON (red) grid cells in the GISS-SST ensemble for Mexico. All variables are expressed in terms of absolute units: precipitation (mm/day; red and blue lines; a), precipitation plus irrigation over IRR grid cells (mm/day; green lines; a), near-surface soil moisture (mm; b), and evaporative fraction (unitless; c). Solid lines indicate the ensemble median, while shading shows the 25th–75th percentile range calculated across the ensemble.

While the evaporative fraction values indicate that both regions occupy moisture-limited evaporative regimes (Figures 12c and 12f), the Eastern Mediterranean is much more arid, with values between 0.24 and 0.34. Even the additional water from irrigation in this region is therefore unlikely to fully satisfy the continuing increases in evaporative demand with warming. This is evidenced by the fact that the cooling response to irrigation is largest and most significant when the evaporative fraction difference is highest at the turn of the 21st century (Figure 8e), while afterwards, the evaporative fraction, and enhanced latent heating associated with irrigation, declines and the cooling effect disappears. The Western Mediterranean, however, occupies intermediate evaporative fraction values where temperature sensitivity to soil moisture is highest, with overall higher water availability that can continue to compensate for increases in evaporative demand and support a significant irrigation cooling effect in the latter half of the 21st century.

3.4.4. Southwest Asia

Southwest Asia is the most arid region in our analysis, with the lowest absolute values of precipitation (Figure 13a), nonirrigated soil moisture (Figure 13b), and evaporative fraction (Figure 13c). As a result, water inputs are dominated by irrigation, which strongly moderates warming (Figure 8f) and soil moisture drying (Figure 9f). Notably, these irrigation effects are strong and persistent out to the end of the 21st century

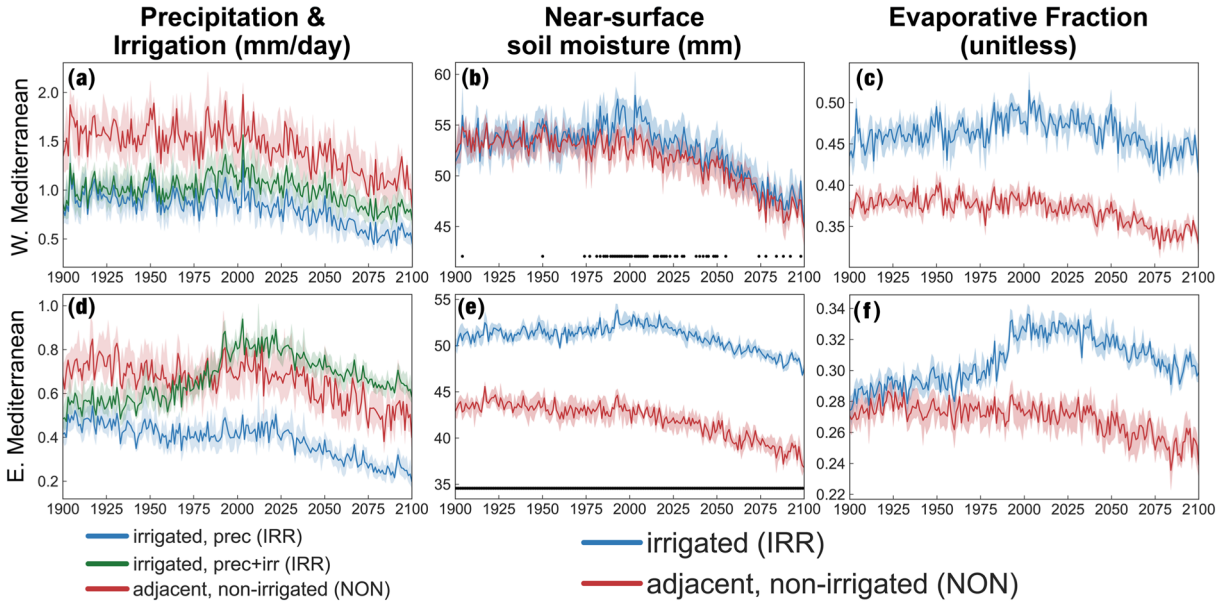

Figure 12. Hydroclimate over IRR (blue and green) and NON (red) grid cells in the GISS-SST ensemble for the Western Mediterranean (a–c) and the Eastern Mediterranean (d–f). All variables are expressed in terms of absolute units: precipitation (mm/day; red and blue lines; a, d), precipitation plus irrigation over IRR grid cells (mm/day; green lines; a, d), near-surface soil moisture (mm; b, e), and evaporative fraction (unitless; c, f). Solid lines indicate the ensemble median, while shading shows the 25th–75th percentile range calculated across the ensemble.

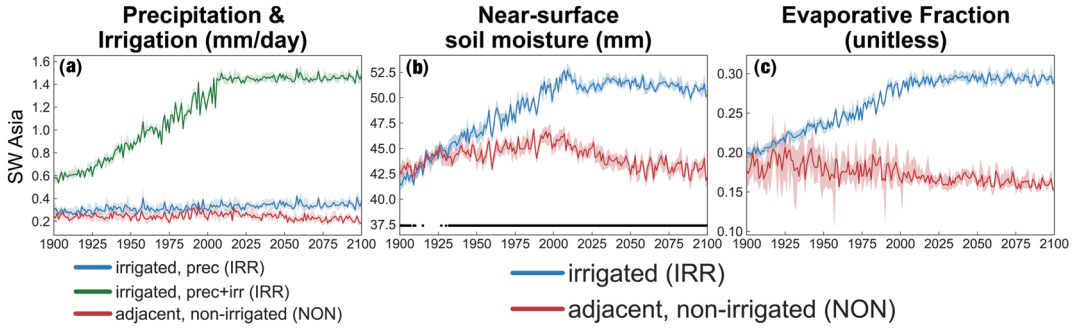

Figure 13. Hydroclimate over IRR (blue and green) and NON (red) grid cells in the GISS-SST ensemble for Southwest Asia. All variables are expressed in terms of absolute units: precipitation (mm/day; red and blue lines; a), precipitation plus irrigation over IRR grid cells (mm/day; green lines; a), near-surface soil moisture (mm; b), and evaporative fraction (unitless; c). Solid lines indicate the ensemble median, while shading shows the 25th–75th percentile range calculated across the ensemble.

because irrigation rates are so large compared to background precipitation and thus are able to maintain significantly higher absolute soil moisture values in the IRR grid cells (Figure 13b). This sustained increase in soil moisture allows for large and sustained increases in evaporative fraction (+0.15) and latent heat fluxes, which effectively moderates the warming out to the end of the 21st century (Figure 8f).

3.4.5. Central and Northern China

Central and Northern China are the two most mesic regions in ModelE, with high precipitation (Figures 14a and 14d) and evaporative fraction (Figures 14c and 14f) values in excess of 0.5, close to the transition between moisture and energy-limited evaporative regimes. Precipitation changes over Central China are small (Figure 14a), but precipitation increases strongly in the 21st century over Northern China (Figure 14d). Despite this increase in precipitation, however, soil moisture actually decreases over NON grid cells in Northern China (Figure 14e), likely a consequence of increased evaporative demand and evapotranspiration in response to atmospheric warming. Over IRR, however, increased precipitation and irrigation cause increases in absolute soil moisture from the twentieth century to the early 21st century (Figure 14e). Even with the 21st century soil moisture drying, soil moisture over IRR grid cells is higher at the end of the 21st

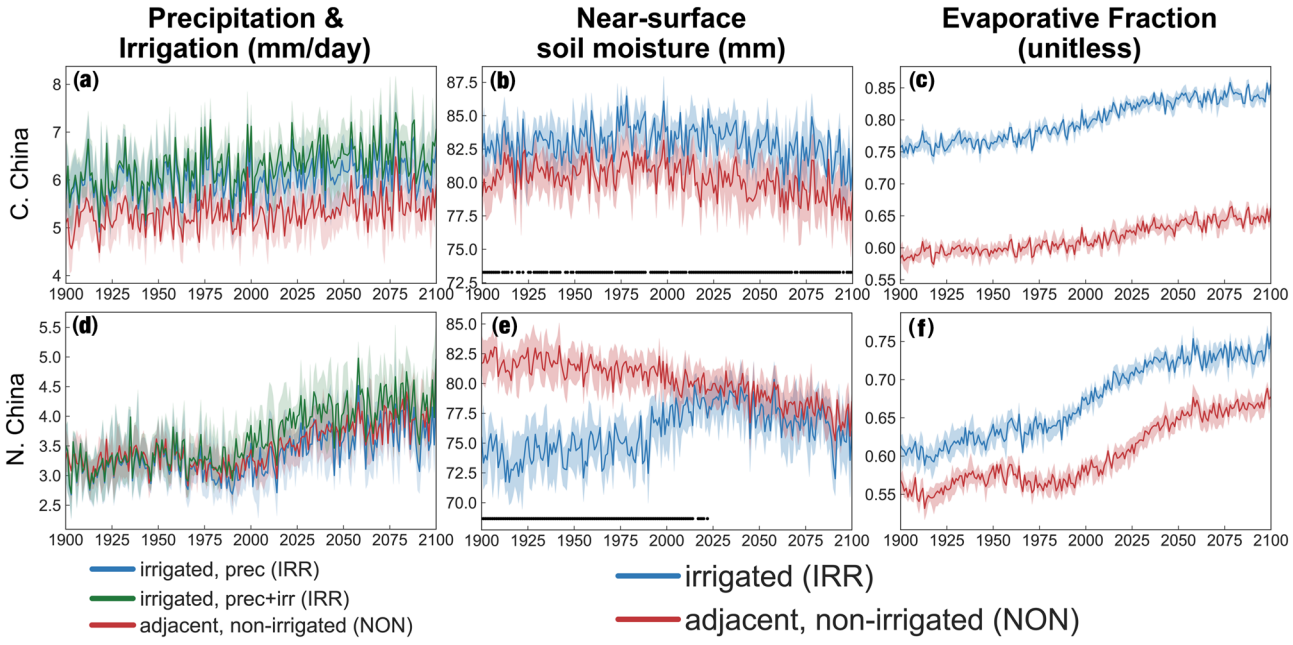

Figure 14. Hydroclimate over IRR (blue and green) and NON (red) grid cells in the GISS-SST ensemble for Central China (a–c) and the Northern China (d–f). All variables are expressed in terms of absolute units: precipitation (mm/day; red and blue lines; a, d), precipitation plus irrigation over IRR grid cells (mm/day; green lines; a, d), near-surface soil moisture (mm; b, e), and evaporative fraction (unitless; c, f). Solid lines indicate the ensemble median, while shading shows the 25th–75th percentile range calculated across the ensemble.

century compared to the early twentieth baseline, which manifests as a positive difference in soil moisture anomalies (Figure 9h). Over Central China, irrigation and precipitation contribute to higher absolute soil moisture over the IRR versus NON grid cells for the entire period of simulation (Figure 14b). Relative changes in soil moisture, however, are similar in both IRR and NON, even if the absolute differences are large, resulting in limited irrigation effects on soil moisture trends in this region (Figure 9g).

Irrigation significantly dampens warming trends in both Central and Northern China (Figures 8g and 8h), an ostensibly surprising result given that these areas occupy borderline energy-limited evaporative regimes (Figures 14c and 14f) where temperature responses to irrigation would be expected to be weak. However, warming increases evaporative demand in the atmosphere, relaxing energy constraints on evapotranspiration (Cook et al., 2014; Scheff & Frierson, 2013), which increases the sensitivity of evapotranspiration in these regions to surface moisture availability. With warming-driven increases in evaporative demand, irrigation results in sustained increases to evaporative fraction and latent heating, which diminishes warming over IRR versus NON grid cells, especially over Central China (Figure 8g). Over Northern China, this irrigation cooling effect is transient and strongest in the early 21st century (Figure 8h). This may be due, in part, to the strong wetting trend in precipitation over both IRR and NON grid cells, adding another source of increased moisture availability on top of irrigation and potentially overcompensating for any increases in evaporative demand, diminishing the benefits of irrigation for temperature in this region.

4. Discussion and Conclusions

Changes in anthropogenic greenhouse gas forcing will dominate the global evolution of the climate system over the next century. Locally, however, climate change will be filtered through a variety of important processes operating at smaller scales that may amplify or attenuate regional impacts. Here, we investigated the capacity for irrigation to modulate future warming and soil moisture drying caused by increases in greenhouse gas forcing over the 21st century. Using a large ensemble simulation with the GISS climate model (ModelE), we found that maintaining current irrigation rates into the future will continue to attenuate climate change impacts on SAT and soil moisture in regions like the Mediterranean, Mexico, and Southwest Asia, even in the face of increasing greenhouse forcing and warming. However, we found that these regional climate responses to irrigation are highly sensitive to the mean state of, and changes in, the local hydroclimate regime.

For soil moisture, irrigation effects manifest most strongly in regions where climate change causes soil moisture drying in the future, through either declines in precipitation (e.g., Western Mediterranean) or increases in evaporative losses from increased precipitation and higher evaporative demand (e.g., Northern China). Our study demonstrates that sustaining current irrigation rates could significantly buffer, though likely not completely prevent, soil moisture losses in the future in these areas. For temperatures, irrigation effects will likely be most significant in regions where evapotranspiration is currently limited by soil water availability (e.g., Mexico) or will become increasingly so in the future (e.g., Central China) through warming-induced increases in evaporative demand. In some regions, however, future drying may be so severe (e.g., the Eastern Mediterranean) that current irrigation rates will be unable to compensate for expected moisture losses by the end of the 21st century, meaning that any irrigation benefit will be temporary. Thus, while irrigation will likely remain a significant anthropogenic climate forcing that should be considered when assessing regional climate change impacts and adaptation policies centered around agriculture and land use development (e.g., Hirsch et al., 2017; Seneviratne et al., 2018), the magnitude of its impacts will likely be highly regionally dependent.

This work is intended as a broad sensitivity study to assess the potential for irrigation to continue ameliorating climate impacts against a steadily increasing background warming trend. Our results and conclusions therefore need to be framed within several important uncertainties and caveats. First, we use an ensemble simulation of a single climate model, ModelE, which may bias our results in important ways. There are often large differences across climate models in land-atmosphere coupling strength (Berg & Sheffield, 2018; Koster et al., 2004) and regional precipitation responses to warming (Knutti & Sedlacek, 2013). All these factors can affect the magnitude and timing of irrigation effects on climate within models (e.g., Boucher et al., 2004; Puma & Cook, 2010; Sacks et al., 2009). In the case of precipitation, 21st century JJA precipitation trends in the GISS-SST ensemble are largely consistent with other CMIP5 models that were also forced with

RCP 8.5 (Knutti & Sedlacek, 2013). This includes drying over Mexico and the Western and Eastern Mediterranean, wetting over Central and Northern China, and weaker (and less robust) trends over Western North America, the Central Plains, and Southwest Asia.

We also only considered one forcing scenario in our ensemble, RCP 8.5. This represents one of the highest greenhouse gas forcing pathways available, which generated a strong and transient warming over the 21st century that allowed us to evaluate irrigation effects across a range of warming levels. However, it is possible that irrigation effects may manifest differently in lower forcing scenarios, such as RCP 4.5, including those that stabilize climate toward the end of the 21st century. In addition to changes in global radiative forcing from greenhouse gas concentrations, RCP 8.5 also includes its own land use scenario that could also affect the interpretation of our results. Land cover change in RCP 8.5, however, is primarily characterized by widespread deforestation and expansion of crop lands in the tropics and subtropics. For most of our regions (Western North America, Central Plains, Eastern Mediterranean, Southwest Asia, Central China, and Northern China), which occupy the Northern Hemisphere midlatitudes, land cover changes were minimal over the 21st century, typically less than 10–20%. In regions that saw more substantial shifts (cropland expansion in Mexico and declines in crop areas in the Western Mediterranean), these land cover changes were spatially extensive, affecting both IRR and NON grid cells. The effect of land cover changes on IRR and NON differences in our analysis is therefore likely relatively minor.

The representation of irrigation within ModelE, and climate models in general, is another key uncertainty (Mathur & AchutaRao, 2019). This includes both how irrigation water is applied to the landscape and the specific irrigation scenario we chose for the 21st century. Two major weaknesses in the implementation of irrigation in ModelE are (1) groundwater for irrigation is treated as an effectively unlimited resource and (2) irrigation is applied to the full vegetated area of the grid cells, rather than just the agricultural fraction. As a consequence, the total land area irrigated is larger in ModelE compared to the original IWD data set, even though the total volume of irrigation water itself is the same, and there is always enough water to meet the demand, factors that together could lead to an overestimate of irrigation effects on climate. While this is suboptimal and largely constrained by limitations in the model architecture (e.g., there is no separate agricultural soil tile or column in ModelE), we also note that there are no defined standards or established state-of-the-art implementations for irrigation treatments in climate models. For example, in the latest version of the Community Earth System Model (CESM2 Danabasoglu et al., 2020), irrigation water is first sourced from river water storage; if the demand cannot be satisfied from these sources, water is then taken from the oceans (Lawrence et al., 2018). The implicit assumption in CESM2 is thus that this water must come from desalinization, when in fact irrigation water is overwhelmingly sourced from surface freshwater and groundwater sources (Siebert et al., 2010; Thenkabail et al., 2009). Irrigation in CESM2 also depends solely on crop water demands (Lawrence et al., 2018), ignoring potential nonphysical constraints that are included within the offline calculated IWD estimates (Wada et al., 2014). This can lead to issues over some regions like South Asia, where in CESM2, the model-based crop planting dates incorrectly bias planting and irrigation over much of the region toward spring, resulting in a warm bias during other seasons in the region (Danabasoglu et al., 2020). Integrating irrigation into climate models thus remains a challenging task for any modeling group, and advances in this regard would strongly benefit from more careful model representations of actual irrigation practices in terms of timing, source of water, method of application, and decision making.

We also acknowledge that our future irrigation scenario, where modern irrigation rates are effectively maintained through to the end of the 21st century regardless of any changes in water resources, may be overly optimistic, especially in light of current constraints on recent irrigation expansion and intensification (Elliott et al., 2014; Faurès et al., 2002; Turral et al., 2011). There are, in fact, good reasons to expect that irrigation will decline in many regions, as water demands increase (e.g., with increased population and climate change) and nonrenewable water resources (e.g., groundwater) are depleted. Future work should therefore consider alternative irrigation scenarios, including those where irrigation is more strongly constrained by changes in water availability, and improved assessments of what would actually be required to maintain or increase irrigation in a rapidly warming world.

Lastly, while current irrigation may incidentally serve to help diminish greenhouse gas-forced climate changes now and in the future, we nonetheless caution against its direct promotion as a climate adaptation

strategy. Our study highlights the importance of irrigation as a regional climate forcing, but the immensity of water that must be added to maintain these irrigation rates is nontrivial. Current irrigation demands are often satisfied at the expense of water resources elsewhere through groundwater depletion (Famiglietti, 2014; Rodell et al., 2009; Wada et al., 2010) or impacts on return flows (e.g., Grafton et al., 2018). Such water resource abstractions are already unsustainable in many regions, and promoting irrigation as a mitigation strategy could work against the development of alternative cropping systems for climate adaptation (e.g., climate smart agriculture Hirsch et al., 2018; Lipper et al., 2014). Thus, while irrigation will likely continue to have important impacts on regional climate in the future, it will not serve as a sufficient replacement for the direct mitigation of greenhouse gas emissions.

Acknowledgments

B. I. Cook, R. Seager, A. P. Williams, and M. J. Puma were all supported for this work by the National Aeronautics and Space Administration (NASA) Modeling, Analysis, and Prediction Program (NASA 80NSSC17K0265). A. P. Williams was also supported by the National Science Foundation (NSF) Paleo Perspectives on Climate Change (AGS 1703029). Resources supporting this work were provided by the NASA High-End Computing (HEC) Program through the NASA Center for Climate Simulation (NCCS) at Goddard Space Flight Center. We also thank three anonymous reviewers for their helpful comments that greatly improved our manuscript. Lamont contribution #8412. GISS-SST ensemble is freely available online (at https://dester.ldeo.columbia.edu:81/SOURCES/.NASA/).

References

Bassi, N. (2014). Assessing potential of water rights and energy pricing in making groundwater use for irrigation sustainable in India. *Water Policy*, *16*(3), 442–453. https://doi.org/10.2166/wp.2013.123

Berg, A., & Sheffield, J. (2018). Soil moisture–evapotranspiration coupling in CMIP5 Models: Relationship with simulated climate and projections. *Journal of Climate*, *31*(12), 4865–4878. https://doi.org/10.1175/JCLI-D-17-0757.1

Bonfils, C., & Lobell, D. (2007). Empirical evidence for a recent slowdown in irrigation-induced cooling. *Proceedings of the National Academy of Sciences*, *104*(34), 13,582–13,587. https://doi.org/10.1073/pnas.0700144104

Boucher, O., Myhre, G., & Myhre, A. (2004). Direct human influence of irrigation on atmospheric water vapour and climate. *Climate Dynamics*, *22*(6), 597–603. https://doi.org/10.1007/s00382-004-0402-4

Chen, L., & Dirmeyer, P. A. (2019). Global observed and modelled impacts of irrigation on surface temperature. *International Journal of Climatology*, *39*, 2587–2600. https://doi.org/10.1002/joc.5973

Cook, B. I., Puma, M. J., & Krakauer, N. Y. (2011). Irrigation induced surface cooling in the context of modern and increased greenhouse gas forcing. *Climate Dynamics*, *37*(7-8), 1587–1600. https://doi.org/10.1007/s00382-010-0932-x

Cook, B. I., Seager, R., Williams, A. P., Puma, M. J., McDermid, S., Kelley, M., & Nazarenko, L. (2019). Climate change amplification of natural drought variability: The historic mid-twentieth-century North American drought in a warmer world. *Journal of Climate*, *32*(17), 5417–5436. https://doi.org/10.1175/JCLI-D-18-0832.1

Cook, B. I., Shukla, S. P., Puma, M. J., & Nazarenko, L. S. (2015). Irrigation as an historical climate forcing. *Climate Dynamics*, *44*(5), 1715–1730. https://doi.org/10.1007/s00382-014-2204-7

Cook, B. I., Smerdon, J. E., Seager, R., & Coats, S. (2014). Global warming and 21st century drying. *Climate Dynamics*, *43*(9-10), 2607–2627. https://doi.org/10.1007/s00382-014-2075-y

Danabasoglu, G., Lamarque, J. F., Bacmeister, J., Bailey, D. A., DuVivier, A. K., Edwards, J, et al. (2020). The Community Earth System Model Version 2 (CESM2). *Journal of Advances in Modeling Earth Systems*, *12*, e01916. https://doi.org/10.1029/2019MS001916

de Vrese, P., Hagemann, S., & Claussen, M. (2016). Asian irrigation, African rain: Remote impacts of irrigation. *Geophysical Research Letters*, *43*, 3737–3745. https://doi.org/10.1002/2016GL068146

DeAngelis, A., Dominguez, F., Fan, Y., Robock, A., Kustu, M. D., & Robinson, D. (2010). Evidence of enhanced precipitation due to irrigation over the Great Plains of the United States. *Journal of Geophysical Research*, *115*, D15115. https://doi.org/10.1029/2010JD013892

Elliott, J., Deryng, D., Müller, C., Frieler, K., Konzmann, M., Gerten, D., et al. (2014). Constraints and potentials of future irrigation water availability on agricultural production under climate change. *Proceedings of the National Academy of Sciences*, *111*(9), 3239. https://doi.org/10.1073/pnas.1222474110

Eyring, V., Bony, S., Meehl, G. A., Senior, C., Stevens, B., Stouffer, R. J., & Taylor, K. E. (2016). Overview of the Coupled Model Intercomparison Project Phase 6 (CMIP6) experimental design and organisation. *Geoscientific Model Development Discussions*, *8*, 1937–1958. https://doi.org/10.5194/gmdd-8-10539-2015

Famiglietti, J. S. (2014). The global groundwater crisis. *Nature Climate Change*, *4*, 945–948. https://doi.org/10.1038/nclimate2425

Faurès, J. M., Hoogeveen, J., & Bruinsma, J. (2002). *The FAO irrigated area forecast for 2030*. Rome, Italy: Food and Agriculture Organization of the United Nations.

Federer, C. A., Vörösmarty, C., & Fekete, B. (2003). Sensitivity of annual evaporation to soil and root properties in two models of contrasting complexity. *Journal of Hydrometeorology*, *4*, 1276–1290. https://doi.org/10.1175/1525-7541(2003)004<1276:SOAETS>2.0.CO;2

Grafton, R. Q., Williams, J., Perry, C. J., Molle, F., Ringler, C., Steduto, P., et al. (2018). The paradox of irrigation efficiency. *Science*, *361*(6404), 748–750. https://doi.org/10.1126/science.aat9314

Grogan, D. S., Wisser, D., Prusevich, A., Lammers, R. B., & Frolking, S. (2017). The use and re-use of unsustainable groundwater for irrigation: A global budget. *Environmental Research Letters*, *12*(3), 034,017. https://doi.org/10.1088/1748-9326/aa5fb2

Guimberteau, M., Laval, K., Perrier, A., & Polcher, J. (2012). Global effect of irrigation and its impact on the onset of the Indian summer monsoon. *Climate Dynamics*, *39*(6), 1329–1348. https://doi.org/10.1007/s00382-011-1252-5

Han, S., & Yang, Z. (2013). Cooling effect of agricultural irrigation over Xinjiang, Northwest China from 1959 to 2006. *Environmental Research Letters*, *8*(2), 024,039. https://doi.org/10.1088/1748-9326/8/2/024039

Hirsch, A. L., Prestele, R., Davin, E. L., Seneviratne, S. I., Thiery, W., & Verburg, P. H. (2018). Modelled biophysical impacts of conservation agriculture on local climates. *Global Change Biology*, *24*(10), 4758–4774. https://doi.org/10.1111/gcb.14362

Hirsch, A. L., Wilhelm, M., Davin, E. L., Thiery, W., & Seneviratne, S. I. (2017). Can climate-effective land management reduce regional warming? *Journal of Geophysical Research: Atmospheres*, *122*(4), 2269–2288. https://doi.org/10.1002/2016JD026125

Kay, J. E., Deser, C., Phillips, A., Mai, A., Hannay, C., Strand, G., et al. (2014). The Community Earth System Model (CESM) large ensemble project: A community resource for studying climate change in the presence of internal climate variability. *Bulletin of the American Meteorological Society*, *96*(8), 1333–1349. https://doi.org/10.1175/BAMS-D-13-00255.1

Kim, Y., Moorcroft, P. R., Aleinov, I., Puma, M. J., & Kiang, N. Y. (2015). Variability of phenology and fluxes of water and carbon with observed and simulated soil moisture in the Ent Terrestrial Biosphere Model (Ent TBM version 1.0.1.0.0). *Geoscientific Model Development*, *8*(12), 3837–3865. https://doi.org/10.5194/gmd-8-3837-2015

Knutti, R., & Sedlacek, J. (2013). Robustness and uncertainties in the new CMIP5 climate model projections. *Nature Climate Change*, *3*(4), 369–373. https://doi.org/10.1038/nclimate1716

Koster, R. D., Dirmeyer, P. A., Guo, Z., Bonan, G., Chan, E., Cox, P., et al. (2004). Regions of strong coupling between soil moisture and precipitation. *Science*, *305*(5687), 1138–1140. https://doi.org/10.1126/science.1100217

Koster, R. D., Schubert, S. D., & Suarez, M. J. (2009). Analyzing the concurrence of meteorological droughts and warm periods, with implications for the determination of evaporative regime. *Journal of Climate*, *22*(12), 3331–3341. https://doi.org/10.1175/2008JCLI2718.1

Kueppers, L., Snyder, M., & Sloan, L. (2007). Irrigation cooling effect: Regional climate forcing by land-use change. *Geophysical Research Letters*, *34*, L03703. https://doi.org/10.1029/2006GL028679

Kumar, S., Dirmeyer, P. A., Merwade, V., DelSole, T., Adams, J. M., & Niyogi, D. (2013). Land use/cover change impacts in CMIP5 climate simulations: A new methodology and 21st century challenges. *Journal of Geophysical Research: Atmospheres*, *118*, 6337–6353. https://doi.org/10.1002/jgrd.50463

Lawrence, D., Fisher, R., Koven, C., Oleson, K., Swenson, S., Vertenstein, M., et al. (2018). Technical description of version 5.0 of the Community Land Model (CLM) (*257*): National Center for Atmospheric Research (NCAR), NCAR Technical Note NCAR/TN-478+ STR.

Lejeune, Q., Seneviratne, S. I., & Davin, E. L. (2017). Historical land-cover change impacts on climate: Comparative assessment of lucid and CMIP5 multimodel experiments. *Journal of Climate*, *30*(4), 1439–1459. https://doi.org/10.1175/JCLI-D-16-0213.1

Levidow, L., Zaccaria, D., Maia, R., Vivas, E., Todorovic, M., & Scardigno, A. (2014). Improving water-efficient irrigation: Prospects and difficulties of innovative practices. *Agricultural Water Management*, *146*, 84–94. https://doi.org/10.1016/j.agwat.2014.07.012

Lipper, L., Thornton, P., Campbell, B. M., Baedeker, T., Braimoh, A., Bwalya, M., et al. (2014). Climate-smart agriculture for food security. *Nature Climate Change*, *4*, 1068–1072. https://doi.org/10.1038/nclimate2437

Lo, M. H., & Famiglietti, J. S. (2013). Irrigation in California's Central Valley strengthens the southwestern U.S. water cycle. *Geophysical Research Letters*, *40*, 301–306. https://doi.org/10.1002/grl.50108

Lobell, D., & Bonfils, C. (2008). The effect of irrigation on regional temperatures: A spatial and temporal analysis of trends in California, 1934–2002. *Journal of Climate*, *21*(10), 2063–2071.

Lobell, D. B., Bonfils, C., & Faurès, J. M. (2008). The role of irrigation expansion in past and future temperature trends. *Earth Interactions*, *12*(3), 1–11. https://doi.org/10.1175/2007EI241.1

Lobell, D. B., Bonfils, C. J., Kueppers, L. M., & Snyder, M. A. (2008). Irrigation cooling effect on temperature and heat index extremes. *Geophysical Research Letters*, *35*, L09705. https://doi.org/10.1029/2008GL034145

Mahmood, R., Foster, S. A., Keeling, T., Hubbard, K. G., Carlson, C., & Leeper, R. (2006). Impacts of irrigation on 20th century temperature in the northern Great Plains. *Global and Planetary Change*, *54*(1), 1–18. https://doi.org/10.1016/j.gloplacha.2005.10.004

Mahmood, R., Keeling, T., Foster, S. A., & Hubbard, K. G. (2013). Did irrigation impact 20th century air temperature in the High Plains aquifer region? *Applied Geography*, *38*, 11–21. https://doi.org/10.1016/j.apgeog.2012.11.002

Mathur, R., & AchutaRao, K. (2019). A modelling exploration of the sensitivity of the India's climate to irrigation. *Climate Dynamics*, *54*, 1851–1872. https://doi.org/10.1007/s00382-019-05090-8

Nazemi, A., & Wheater, H. S. (2015). On inclusion of water resource management in Earth system models—Part 1: Problem definition and representation of water demand. *Hydrology and Earth System Sciences*, *19*(1), 33–61. https://doi.org/10.5194/hess-19-33-2015

Nocco, M. A., Smail, R. A., & Kucharik, C. J. (2019). Observation of irrigation-induced climate change in the Midwest United States. *Global Change Biology*, *25*, 3472–3484. https://doi.org/10.1111/gcb.14725

Portmann, F. T., Siebert, S., & Döll, P. (2010). MIRCA2000—Global monthly irrigated and rainfed crop areas around the year 2000: A new high-resolution data set for agricultural and hydrological modeling. *Global Biogeochemical Cycles*, *24*, GB1011. https://doi.org/10.1029/2008GB003435

Puma, M. J., & Cook, B. I. (2010). Effects of irrigation on global climate during the 20th century. *Journal of Geophysical Research*, *115*, D16120. https://doi.org/10.1029/2010JD014122

Rayner, N. A., Parker, D. E., Horton, E. B., Folland, C. K., Alexander, L. V., Rowell, D. P., et al. (2003). Global analyses of sea surface temperature, sea ice, and night marine air temperature since the late nineteenth century. *Journal of Geophysical Research*, *108*(D14), 4407. https://doi.org/10.1029/2002JD002670

Rodell, M., Velicogna, I., & Famiglietti, J. S. (2009). Satellite-based estimates of groundwater depletion in India. *Nature*, *460*(7258), 999–1002. https://doi.org/10.1038/nature08238

Sacks, W. J., Cook, B. I., Buenning, N., Levis, S., & Helkowski, J. H. (2009). Effects of global irrigation on the near-surface climate. *Climate Dynamics*, *33*(2), 159–175. https://doi.org/10.1007/s00382-008-0445-z

Scheff, J., & Frierson, D. M. W. (2013). Scaling potential evapotranspiration with greenhouse warming. *Journal of Climate*, *27*, 1539–1558. https://doi.org/10.1175/JCLI-D-13-00233.1

Schewe, J., Heinke, J., Gerten, D., Haddeland, I., Arnell, N. W., Clark, D. B., et al. (2014). Multimodel assessment of water scarcity under climate change. *Proceedings of the National Academy of Sciences*, *111*(9), 3245. https://doi.org/10.1073/pnas.1222460110

Seneviratne, S. I., Phipps, S. J., Pitman, A. J., Hirsch, A. L., Davin, E. L., Donat, M. G., et al. (2018). Land radiative management as contributor to regional-scale climate adaptation and mitigation. *Nature Geoscience*, *11*(2), 88–96. https://doi.org/10.1038/s41561-017-0057-5

Shukla, S. P., Puma, M. J., & Cook, B. I. (2014). The response of the South Asian Summer Monsoon circulation to intensified irrigation in global climate model simulations. *Climate Dynamics*, *42*, 21–36. https://doi.org/10.1007/s00382-013-1786-9

Siebert, S., Burke, J., Faures, J. M., Frenken, K., Hoogeveen, J., Döll, P., & Portmann, F. T. (2010). Groundwater use for irrigation—A global inventory. *Hydrology and Earth System Sciences*, *14*(10), 1863–1880. https://doi.org/10.5194/hess-14-1863-2010

Siebert, S., & Döll, P. (2010). Quantifying blue and green virtual water contents in global crop production as well as potential production losses without irrigation. *Journal of Hydrology*, *384*(3), 198–217. https://doi.org/10.1016/j.jhydrol.2009.07.031

Siebert, S., Döll, P., Feick, S., & Hoogeveen, J. (2005). *Global map of irrigated areas version 2.2*. Frankfurt, Germany: Johann Wolfgang Goethe University.

Siebert, S., Döll, P., Hoogeveen, J., Faures, J. M., Frenken, K., & Feick, S. (2005). Development and validation of the global map of irrigation areas. *Hydrology and Earth System Sciences*, *9*(5), 535–547. https://doi.org/10.5194/hess-9-535-2005

Siebert, S., Kummu, M., Porkka, M., Döll, P., Ramankutty, N., & Scanlon, B. R. (2015). A global data set of the extent of irrigated land from 1900 to 2005. *Hydrology and Earth System Sciences*, *19*(3), 1521–1545. https://doi.org/10.5194/hess-19-1521-2015

Singh, D., McDermid, S. P., Cook, B. I., Puma, M. J., Nazarenko, L., & Kelley, M. (2018). Distinct influences of land cover and land management on seasonal climate. *Journal of Geophysical Research: Atmospheres*, *123*, 12,017–12,039. https://doi.org/10.1029/2018JD028874

Thenkabail, P. S., Biradar, C. M., Noojipady, P., Dheeravath, V., Li, Y., Velpuri, M., et al. (2009). Global Irrigated Area Map (GIAM), derived from remote sensing, for the end of the last millennium. *International Journal of Remote Sensing*, *30*(14), 3679–3733. https://doi.org/10.1080/01431160802698919

Thiery, W., Davin, E. L., Lawrence, D. M., Hirsch, A. L., Hauser, M., & Seneviratne, S. I. (2017). Present-day irrigation mitigates heat extremes. *Journal of Geophysical Research: Atmospheres*, *122*, 1403–1422. https://doi.org/10.1002/2016JD025740

Thiery, W., Visser, A. J., Fischer, E. M., Hauser, M., Hirsch, A. L., Lawrence, D. M., et al. (2020). Warming of hot extremes alleviated by expanding irrigation. *Nature Communications*, *11*(1), 290. https://doi.org/10.1038/s41467-019-14075-4

Turral, H., Burke, J. J., & Faurès, J. M. (2011). Climate change, water and food security (*Water Report No. 36*). Rome, Italy: Food and Agriculture Organization of the United Nations.

Vörösmarty, C. J., Federer, C. A., & Schloss, A. L. (1998). Potential evaporation functions compared on US watersheds: Possible implications for global-scale water balance and terrestrial ecosystem modeling. *Journal of Hydrology*, *207*(3-4), 147–169. https://doi.org/10.1016/S0022-1694(98)00109-7

Wada, Y., van Beek, L. P. H., van Kempen, C. M., Reckman, J. W. T. M., Vasak, S., & Bierkens, M. F. P. (2010). Global depletion of groundwater resources. *Geophysical Research Letters*, *37*, L20402. https://doi.org/10.1029/2010GL044571

Wada, Y., Wisser, D., & Bierkens, M. F. P. (2014). Global modeling of withdrawal, allocation and consumptive use of surface water and groundwater resources. *Earth System Dynamics*, *5*(1), 15–40. https://doi.org/10.5194/esd-5-15-2014

Wada, Y., Wisser, D., Eisner, S., Flörke, M., Gerten, D., Haddeland, I., et al. (2013). Multi-model projections and uncertainties of irrigation water demand under climate change. *Geophysical Research Letters*, *40*, 4626–4632. https://doi.org/10.1002/grl.50686

Wisser, D., Fekete, B. M., Vorosmarty, C. J., & Schumann, A. (2010). Reconstructing 20th century global hydrography: A contribution to the Global Terrestrial Network-Hydrology (GTN-H). *Hydrology and Earth System Sciences*, *14*, 1–24. https://doi.org/10.5194/hess-14-1-2010

Yang, Z., Dominguez, F., Zeng, X., Hu, H., Gupta, H., & Yang, B. (2017). Impact of irrigation over the California Central Valley on regional climate. *Journal of Hydrometeorology*, *18*(5), 1341–1357. https://doi.org/10.1175/JHM-D-16-0158.1

Yang, Q., Huang, X., & Tang, Q. (2020). Irrigation cooling effect on land surface temperature across China based on satellite observations. *Science of The Total Environment*, *705*, 135,984. https://doi.org/10.1016/j.scitotenv.2019.135984